Disruption of GCN2 pathway aggravates vascular and parenchymal remodelling during pulmonary fibrosis.

Diana Santos-Ribeiro[1], Marylène Lecocq[1], Michèle De Beukelaer[2], Stijn Verleden[3], Caroline Bouzin[2], Jérôme Ambroise[4], Peter Dorfmuller[5], Yousef Yakoub[6], François Huaux[6], Rozenn Quarck[7], Harry Karmouty-Quintana[8], Maria-Rosa Ghigna[9], Juliette Bignard[10], Sophie Nadaud[10], Florent Soubrier[10], Sandrine Horman[11], Frederic Perros[12], Laurent Godinas[7*], Charles Pilette[1,13*]

1. Institute of Experimental and Clinical Research (IREC), Pneumology, ENT and Dermatology, Université catholique de Louvain (UCL), Brussels, Belgium.
2. Institute of Experimental and Clinical Research (IREC), Imaging Platform (2IP), Université catholique de Louvain (UCL), Brussels, Belgium.
3. Laboratory of Respiratory Diseases & Thoracic Surgery (BREATHE), Department of Chronic Diseases & Metabolism (CHROMETA), KU Leuven – University of Leuven, Leuven, Belgium.
4. Institute of Experimental and Clinical Research (IREC), Centre de Technologies Moléculaires Appliquées (CTMA), Université catholique de Louvain (UCL), Brussels, Belgium.
5. Department of Pathology, University of Giessen and Marburg Lung Center (UGMLC), Justus- Liebig University Giessen, German Center for Lung Research (DZL), Giessen, Germany.
6. Institute of Experimental and Clinical Research (IREC), Louvain Center for Toxicology and Applied Pharmacology, Université catholique de Louvain (UCL), Brussels, Belgium.
7. Clinical Department of Respiratory Diseases, University Hospitals and Laboratory of Respiratory Diseases & Thoracic Surgery (BREATHE), Department of Chronic Diseases & Metabolism (CHROMETA), KU Leuven – University of Leuven, Leuven, Belgium.

8. Department of Biochemistry and Molecular Biology, and Divisions of Critical Care, Pulmonary and Sleep Medicine, Department of Internal Medicine, The University of Texas Health Science Center at Houston, Texas, USA.
9. Université Paris-Saclay, Faculté de Médecine, Le Kremlin-Bicêtre, France; Department of Pathology, Hôpital Marie Lannelongue, 92350 Le Plessis-Robinson, France; INSERM UMR_S 999, Hôpital Marie Lannelongue, Le Plessis Robinson, France.
10. UMR_S 1166-ICAN, INSERM ; Sorbonne Université, Paris, France.
11. Institute of Experimental and Clinical Research (IREC), Cardiovascular Research Unit, Université catholique de Louvain (UCL), Brussels, Belgium.
12. Université Paris-Saclay, Faculté de Médecine, Le Kremlin-Bicêtre, France; AP-HP, Centre de Référence de l'Hypertension Pulmonaire, Service de Pneumologie et Soins Intensifs Respiratoires, Hôpital Bicêtre, Le Kremlin-Bicêtre, France; INSERM UMR_S 999, Hôpital Marie Lannelongue, Le Plessis Robinson, France.
13. Cliniques universitaires St-Luc, Dept. of Pneumology, Brussels, Belgium.

* Contributed equally

Corresponding Author:

Charles Pilette

Institute of Experimental and Clinical Research (IREC)

Avenue Hippocrate 54 Bte B1.54.04 Bernard +3

1200 Brussels –Belgium

Tel: 0032(0)27645462

charles.pilette@uclouvain.be

Conflict of Interest Statement

The authors have declared that no conflict of interest exists.

Abstract

Pulmonary fibrosis (PF) and pulmonary hypertension (PH) are chronic diseases of the pulmonary parenchyma and circulation, respectively, which may coexist, but underlying mechanisms remain elusive. Mutations in the GCN2 gene (*EIF2AK4*) were recently associated with pulmonary veno-occlusive disease. This study aims to explore the involvement of the GCN2/eIF2α pathway in the development of PH during PF, in both human disease and in an experimental animal model. Lung tissue from PF patients with or without PH were collected at the time of lung transplantation, and controls were obtained from tumor resection surgery. Experimental lung disease was induced in either male *wild-type* or *EIF2AK4-mutated* Sprague-Dawley rats, randomly receiving a single intratracheal instillation of bleomycin or saline. Hemodynamic studies, as well as organ collection were performed 3 weeks post-instillation. Only significant results ($p<0.05$) are given. In PF lung tissue, GCN2 protein expression was decreased, when compared with controls. GCN2 expression was reduced in $CD31^+$ endothelial cells. In line with human data, GCN2 protein expression was decreased in the lung of bleomycin rats when compared with saline. *EIF2AK4-mutated* rats treated with bleomycin showed increased parenchymal fibrosis (hydroxyproline levels) and vascular remodeling (media wall thickness) as well as increased right ventricular systolic pressure when compared to *wild-type* animals. Our data shows that GCN2 is dysregulated in both human and in an animal model of combined PF+PH. The possibility of a causative implication of GCN2 dysregulation in PF and/or PH development should be further studied.

Word count: 247

Key words: Lung diseases; Vascular disease; Right ventricular dysfunction

Introduction

Pulmonary fibrosis (PF) represents a chronic and progressive disease characterized by extensive tissue remodeling associated with different causing disorders (the most frequent form remaining idiopathic, as referred to as IPF), which induce the activation of fibroblasts into myofibroblasts, leading to an extracellular matrix accumulation (1, 2). The presence of PH affects 29 to 77% of patients with PF, and it correlates with further impairment in functional outcomes (3). Pulmonary hypertension (PH) is a chronic disorder of the pulmonary circulation defined by a mean pulmonary artery pressure (mPAP) superior to 20 mmHg, measured by right heart catheterization at rest (4-6), which often complicates chronic lung diseases (group 3 PH) such as IPF. Whereas anti-fibrotic drugs are now available to treat IPF, the lack of efficacy of pulmonary arterial hypertension (PAH)-specific therapies in patients with PF (7, 8) highlights the need to better understand the cellular and molecular mechanisms - in particular at the endothelial cell level - that underlie the vascular disease in PF patients.

GCN2 (general control nonderepressible 2) is a serine/threonine kinase ubiquitously expressed in eukaryotic cells that belongs to the integrated stress response (ISR) system. GCN2 plays a major role in cellular adaptation to different types of stress, such as amino acid (AA) deprivation, hypoxia, and oxidative stress (9). Upon a stressful stimulus, GCN2 phosphorylates the alpha subunit of the eukaryotic initiation factor 2 (eIF2α) at Ser51, resulting in the inhibition of mRNA translation, consequently reducing overall protein synthesis. This step is not only important to save the cell resources and attenuate its burden, but also to re-direct the cell machinery to the production of proteins implicated in stress recovery, such as activating transcription factor 4 (ATF4). The activation of this pathway can thus induce the expression of a large range of genes involved in protein synthesis but also in other vital cellular functions such as apoptosis, metabolism, redox balance, and autophagy, according to the nature and severity of the stimuli that triggered ISR activation (9).

Biallelic mutations in the gene coding GCN2 (*EIF2AK4*) were shown to be responsible for the hereditary form of pulmonary venous occlusive disease (PVOD), which is characterized by a progressive remodeling of septal and pre-septal veins with accumulation of fibrotic tissue resulting in total occlusion of the lumen (10). Interestingly, histopathological studies of PF lungs also showed occlusive venopathy lesions, even in the more preserved parts of the lung parenchyma (11, 12). In addition, PVOD in both human and rodents was associated with GCN2 downregulation, independently of *EIF2AK4* mutations (13). Furthermore, cross talks exist between GCN2 and important pathways playing a role in the pathophysiology of PF and PH, such as the mTOR (mammalian target of rapamycin) (14) and TGF-β (transforming growth factor beta) (15).

Based on this evidence we hypothesized that GCN2 could regulate key and common elements of pulmonary and vascular homeostasis, and identified in this study the eIF2α kinase GCN2 as a novel player in the development of PF and PH, due to its potential effect on protein synthesis and fibrosis as well as its involvement in PVOD. We measured the expression of key signaling components of GCN2 pathway in carefully selected and characterized patients with PF combined or not with PH, and studied the consequences of GCN2 knockout in an experimental rat model that displays a combined (PF-PH) phenotype.

Methods

Human lung samples

Human lung tissue was collected with patient's agreement and ethical approval by UCL (Ref. protocol "CLARA" 2005/22SEP/149 – update 29/11/2016), Comité de Protection des Personnes Ile-de-France VII (N8CO-08- 003, ID RCB: 2008-A00485-50) and KU Leuven (S51577, S52174 and S55877). Control lung tissue was collected from patients undergoing lung resection surgery due to a solitary lung cancer, at distance of the tumoral site. PF explants were obtained from patients undergoing lung transplantation. Presence of PF was based on

clinical history including lung scanning and confirmed by lung histology, while the presence of additional PH was based on right heart catheterization results.

Animal experiments and Eif2ak4-mutated rats

Animal experiments were performed in agreement with the European Community regulations, followed the recommendations of the *Guide for the Care and Use of Laboratory Animals* (NIH publication No. 85-23, revised 2011, US) and were approved by the local ethical committee for animal research at the UCLouvain (2017/UCL/MD/003). These rats were generated on a SD background by using the Zinc-Finger nuclease method, as previously described (15). A frameshift deletion of 41 base pairs (*Eif2ak4*$_{\Delta 41}$) was introduced in the first exon of the *Eif2ak4* gene. The strain developed can be either monoallelic or biallelic. Rats with 3 weeks-old were genotyped using genomic DNA obtained from ear punches.

Rats weighing approximately 250g were randomly assigned to receive either an intratracheal instillation of 7.5U/kg of bleomycin sulphate (Sanofi) or an equal volume of vehicle (0.9% NaCl, Baxter). Three weeks post-instillation (day 21), animals were submitted to an invasive hemodynamic evaluation, followed by euthanasia and sample collection.

Tissue, cell and molecular readouts

Experimental details, including information on hemodynamic measurements, sample collection, histological and morphometric analyses, multiplex immunofluorescence staining, protein extraction and immunoblotting, ELISA and BCA assays, primary human lung microvascular endothelial cell culture and treatments, and analysis of single cell RNA-seq databases for GCN2/EIF2AK4 mRNA expression, are provided in the online supplement.

Statistical analysis

Statistical analysis was performed using GraphPad Prism 8 and Single-cell RNA-Seq data were analyzed with Seurat R package (16). All graphs are presented as mean±SD and differences with $p<0.05$ were considered statistically significant.

Results

Patients

Table 1 displays the clinical characteristics of the control and PF patients selected for this study. The CTR patients were age-matched with PF and PF-PH patients. Most PF patients displayed idiopathic PF (IPF, 10/13). Lung function indices were altered in both PF and PF-PH patients, without significant between-group difference, whereas mean pulmonary pressure was higher (as per definition of this subgroup) in patients with combined PF-PH (Table 1).

Pulmonary vascular remodeling is present in human PF.

Both groups, PF and PF-PH, displayed mild intimal remodeling in veins under 200µm, as well as fragmentation/duplication of the elastic lamina (Figure 1A). In a semi-quantitative assessment, the majority of the veins found in PF and PF-PH patients scored 1 (PF: 63%, PF-PH: 53%) or 2 (PF: 34%, PF-PH: 43%) for the presence of intimal fibrosis (p=0.1874) (Figure 1B). Remodeling was also observed in pulmonary arteries (PA) with a diameter inferior to 200µm from PF-PH patients, who had increased wall thickness percentage (WT%) when compared to the control group (CTR, p=0.0220), while this was not altered in PF when compared to control (p=0.6482) and PF-PH patients (p=0.1275) (Figure 1C).

GCN2 signaling pathway is dysregulated in human PF lungs.

In lungs from patients with PF compared with CTR, we found a significant decrease in the protein expression of GCN2 (p=0.0432) (Figure 2A) and in the phosphorylation levels of eIF2α at Ser51 (p=0.0430) (Figure 2B), its downstream target, despite total eIF2α expression was increased in PF patients when compared to controls (Supplemental Figure 4). Patients with combined PF-PH showed further decrease in phosphorylated-eIF2α levels when compared with PF without PH (p=0.0090) (Figure 2C). ATF4 protein expression, a main downstream target following eIF2α phosphorylation, remained however unchanged between groups (p=0.2941)

(Figure 2D). Of note, no difference was observed in the protein expression of GCN2 following stratification according to the smoking history of control subjects (smokers versus non-smokers, data not shown).

GCN2 is downregulated in the endothelium of PF lung arteries.

In small pulmonary vessels (<200µm) from CTR patients, immunofluorescence and colocalization studies showed that GCN2 staining localized predominantly in endothelial cells (35±18% of EC expressing GCN2) and to a lesser extent in smooth muscle cells (8±5% SMC expressing GCN2) (Figure 3A). GCN2 staining was significantly reduced in the endothelium of PF and PF-PH patients, as shown by the decreased percentage of GCN2-positive cells among CD31-positive cells (PF: 10±13% and PF-PH: 11±17%) (p=0.007 and p=0.0146, respectively) (Figure 3B). In contrast, no significant difference was observed between groups for the percentage of GCN2-positive cells among smooth muscle cells (PF: 4±6% and PF-PH: 7±9% (p=0.1387 and p=0.6624, respectively) (Figure 3C). A decrease in the overall expression of the endothelium-specific marker CD31 was also noticed in the lung of PF patients when compared with controls (p=0.0449) (Figure 3D).

Analysis of GCN2 (EIF2AK4) gene expression in human lungs at the single cell level

In contrast with the protein level, the transcriptional levels of GCN2/*EIF2AK4* assessed by RT-qPCR in PF lungs showed upregulation of mRNA transcripts as compared to controls (Supplemental Figure 1A). As GCN2 was more specifically regulated in EC from PF lungs (at the protein level, Figure 3), single cell RNA-Sequencing databases from two studies (17, 18) were analysed for *EIF2AK4* expression (Figure 4 and Supplemental Figure 3). A slight up-regulation (log Fold-change <0.1) was observed in lung EC, as well as in smooth muscle or alveolar epithelial cells, in both studies (Figure 4 and Supplemental Figure 3), which was

198 significant in one study (Figure 4). These datasets collectively indicated that GCN2 is
199 downregulated in PF (and PF-PH) through a posttranscriptional mechanism.

200 *GCN2 signaling is dysregulated in an animal model of combined PF-PH.*

201 Rats submitted to bleomycin (BM) displayed decreased GCN2 protein expression in the lung
202 when compared with saline (SL)-treated animals ($p<0.0001$) (Figure 5A), although no
203 difference was observed in the levels of phosphorylated eIF2α between the two groups
204 ($p=0.2831$) (Figure 5B). In addition, also in line with human data, GCN2 mRNA was
205 significantly upregulated in the lungs from rats treated with BM (Supplemental Figure 1B).

206 *GCN2 loss-of-function mutation aggravates bleomycin-induced combined PF-PH.*

207 In order to study the impact of GCN2 dysfunction *in vivo* and ascertain its role in the
208 pathogenesis of parenchymal and vascular remodeling in the lung, we submitted rats with a
209 loss-of-function mutation in the GCN2 gene (*Eif2ak4*, here denoted as GCN2) ($GCN2^{\Delta41/\Delta41}$) to
210 BM. The genotype of $GCN2^{+/+}$, $GCN2^{+/\Delta41}$ and $GCN2^{\Delta41/\Delta41}$ rats was confirmed by PCR
211 analysis of genomic DNA (Figure 6A). To assess the protein levels of GCN2 in the lungs as
212 well as in the right ventricle (RV) (in order to confirm changes in GCN2 expression in extra-
213 pulmonary tissue) of these animals, we performed western blot analysis for GCN2 on lung and
214 heart homogenates from each genotype to confirm the absence of GCN2 expression in
215 $GCN2^{\Delta41/\Delta41}$ rats (Figure 6B).

216 Upon BM instillation, *wild-type* (WT, $GCN2^{+/+}$) animals developed PF as observed by
217 conventional histology (Figure 6D) and confirmed by the increased content of hydroxyproline
218 (OH-proline) within their lungs (SL-$GCN2^{+/+}$ vs BM-$GCN2^{+/+}$: 589±91 vs 1035±369,
219 $p<0.0001$) (Figure 6C). A mild PH was also noticed in those BM-treated WT rats by increases
220 in pulmonary pressure (RVSP, SL-$GCN2^{+/+}$ vs BM-$GCN2^{+/+}$: 29±3 vs 39±5 mmHg, $p<0.0001$)

(Figure 6E), in Fulton's Index (0.2874±0.02 vs 0.4664±0.09, p<0.0001) (Figure 6F), as well as in percentage of fully muscularized arterioles (10±7% vs 43±10%, p<0.0001) (Figure 6G-6H).

GCN2$^{\Delta 41/\Delta 41}$ rats at baseline did not display pulmonary abnormalities when compared to WT animals. After BM treatment, GCN2 mutated rats demonstrated greater lung abnormalities when compared with WT, in terms of increased OH-proline content (BM-GCN2$^{+/+}$ vs BM-GCN2$^{\Delta 41/\Delta 41}$: 1035±369 vs 1535±315, p<0.0001) (Figure 6C) and the occurrence of extensive peribronchial and parenchymal fibrosis, along with the presence of alveolar hemorrhage (Figure 6D). GCN2 mutated rats also displayed increased PH, with increased RVSP (BM-GCN2$^{+/+}$ vs BM-GCN2$^{\Delta 41/\Delta 41}$: 39±5 vs 46±8, p=0.0019) (Figure 6E) and the shift towards increased presence of fully muscularized (FM) in detriment of non-muscularized (NM) microvessels in the lungs (43±10% vs 52±10%, p=0.0280) (Figure 6G-6H). No statistically significant difference was observed between genotypes for the Fulton's index (Figure 6F).

Loss of GCN2 increases TGF-β1 production and pulmonary vascular permeability

Upon BM challenge, a significant increase in total TGF-β1 was observed in bronchoalveolar lavage (BAL) from GCN2$^{\Delta 41/\Delta 41}$ rats (SL-GCN2$^{\Delta 41/\Delta 41}$ vs BM-GCN2$^{\Delta 41/\Delta 41}$: 0.00±0.00 vs 54.63±71.79 pg/mL, p=0.0315) and not in WT animals (Figure 7A). Following the observation of alveolar hemorrhage in the lungs of GCN2$^{\Delta 41/\Delta 41}$ rats (Figure 6D), the pulmonary permeability index (PPI) was calculated, with BM-GCN2$^{\Delta 41/\Delta 41}$ rats showing increased PPI not only in comparison with SL-GCN2$^{\Delta 41/\Delta 41}$ (0.007±0.002 vs 0.013±0.005, p=0.0054), but also in comparison with BM-GCN2$^{+/+}$ (0.008±0.002 vs 0.013±0.005, p=0.0281) (Figure 7B). Consistent with the increase in pulmonary permeability, an important decrease in the expression of ZO-1 (zonula occludens-1) was noticed in the endothelium of small arteries from BM-treated animals in both genotypes (p<0.0001). A trend for decreased ZO-1 was also observed in BM-GCN2$^{\Delta 41/\Delta 41}$ as compared to BM-treated WT rats (p=0.0980) (Figure 7C-7E). In line with human data, animals submitted to BM showed decreased CD31 immunostaining in small

arteries when compared with control, SL-treated lungs in WT (P=0.0054) and in GCN2$^{\Delta 41/\Delta 41}$ (p=0.0002) (Figure 7D-7E).

In vitro inhibition of GCN2 in pulmonary EC and study of lung vascular cells from mutated rats

In EC isolated from human control lungs, inhibition of GCN2 using a selective inhibitor (HY-112654) (Figure 8B), tended to aggravate the endothelial response to BM in terms of TGF-β1 production (Figure 8C) and upregulation of endothelial-to-mesenchymal transition (endoMT) markers such as TWIST (p=0.056). Upregulation of *Il6* mRNA expression and IL-6 release was also observed in BM-treated endothelial cells upon GCN2 inhibition, while this increase was not observed in fibroblasts (MRC5 cell line) (Figure 8E-8F). We also evaluated endoMT markers in lung tissue from rats showing that expression of VE-cadherin, Twist and Snail were not altered in endothelial cells following BM exposure (Supplemental Figure 5). PA smooth muscle cells (PASMC) isolated from rat lungs revealed that cells from mutated animals had a much lower proliferation rate compared with wild type. In addition, the proliferation rate of control cells also decreased upon BM exposure *in vitro* (Supplemental Figure 6). Altogether, these results show that GCN2 loss-of-function alters pulmonary vascular biology, notably by affecting junctional properties and promoting a pro-fibrotic dysregulation of pulmonary EC, while in-depth studies of underlying mechanisms were prevented by the failure of obtaining EC cultures from diseased PF lungs.

Discussion

In this study, the eIF2α kinase GCN2 was identified as a novel player in the development of tissue fibrosis and vascular remodeling in the lung, showing that GCN2 protein expression was decreased in the lungs from patients with PF and PF-PH. This defect was microlocalized in endothelial cells through a post-transcriptional mechanism and knockout of GCN2/*Eif2ak4 in*

vivo, in rats aggravated pulmonary tissue remodeling and pulmonary hypertension following bleomycin-induced injury, providing a link between parenchymal and vascular remodeling through pathways that connect TGF-β signaling, IL-6 upregulation, endothelial cell dysfunction and vascular hyperpermeability.

First, we confirmed the presence and assessed the degree of vascular remodeling, including venous remodeling, in the lungs from both PF and PF-PH patients (12). Both groups displayed mild intimal fibrosis in small veins (ø<200µm), as well as fragmentation and/or duplication of the elastic lamina, with a trend for increased venous remodeling in PF-PH. In addition and in line with previous studies (12, 19, 20), PF-PH patients showed increased arterial remodeling whereas no difference was observed in PF patients not diagnosed with PH, validating histologically the three study groups. Second, the first main finding of this study is the downregulation of GCN2 protein in both human and BM-induced experimental PF. This defect in GCN2, which was further observed in PF-PH in terms of downstream eIF2α phosphorylation, was contrasting with the upregulation of its gene (*EIF2AK4*) transcription indicating that this protein defect might relate to a post-transcriptional mechanism affecting GCN2 mRNA stability. A failure to culture primary lung EC from PF patients and mutated animals prevented, however, to confirm this possibility.

Loss-of-function mutations in the gene coding for GCN2 (*EIF2AK4*) were recently associated with PVOD, an aggressive form of hereditary PH characterized by extensive venous and capillary remodeling. It was further shown that GCN2 is not only absent in the lung from heritable PVOD patients, but it is also downregulated in sporadic PVOD and PAH patients (21) as well as in related animal models (13). Our data shows for the first time that GCN2 signaling is also reduced in human PF and in BM-induced experimental PF-PH in rats, with downregulation of the phosphorylation of eIF2α, the downstream target of GCN2. Despite the fact that total eIF2α protein levels were increased, there was no increase in phospho-eIF2α and

both mutated animals and PF patients showed increased protein (notably collagen) synthesis. In addition, increased eIF2α protein levels indicate increased eIF2α gene expression. The absence of ATF4 upregulation that is expected during PF (22) could further support GCN2 downregulation. Alternatively, it could indicate ATF4-independent mechanisms (23) or compensatory mechanisms activated through other kinases of the ISR family such as PERK, PKR or HRI (9). Unfortunately, and partly due to the intricate interaction between these proteins, it remains unknown if any of these proteins would be compensating for the loss of GCN2 in our animal model. As other members of the pathway, such as PERK and the unfolded protein response (UPR) pathway, have been described in the pathogenesis of lung disease (9, 24), one might consider that disease might arise due to a dysregulation in the ISR pathway itself rather than to a dysregulation in a member of the pathway. Similarly, the absence of alteration in phosphorylated eIF2α noticed in GCN2-mutated and BM-treated rats might also suggest a compensatory activation of ISR kinases such as PERK, which is able to maintain eIF2α phosphorylation in the absence of GCN2 (25).

Eif2ak4-mutated rats (i.e. with a GCN2 loss-of-function mutation, $GCN2^{\Delta 41/\Delta 41}$), similarly to GCN2 KO mice (26, 27), are viable, fertile and exhibit no phenotypic abnormalities under standard housing conditions. These animals were used to demonstrate the role of GCN2 *in vivo* in a model of combined PF-PH induced by a single dose of BM (28-30). In this model, GCN2 protein expression was downregulated in the lung, as previously observed in mitomycin and monocrotaline-induced experimental PH (13). *Eif2ak4*-mutated rats showed an aggravated response to BM in comparison to WT animals, developing much more severe peribronchial and parenchymal fibrotic lesions. It was similarly shown that $GCN2^{-/-}$ mice were more prone to develop post-injury liver necrosis, inflammation and fibrosis (31). A first possible mechanism of tissue fibrosis in the presence of GCN2 disruption relates to a direct activation of collagen synthesis by fibroblasts. Thus, it was shown that human lung fibroblasts deprived of amino

acids decrease their production of type I collagen (32, 33). These studies did not correlate their findings with GCN2 activation, but GCN2 is required for the adaptation to amino acid deficiency *in vitro* (34, 35) and *in vivo* (36). A second possibility relates to inflammation that plays a role during PF (37) and PH (38), with previous studies showing that GCN2 not only reduces autoimmune reactivity (39) but also suppresses (in the intestine) inflammation via the stimulation of autophagy and sequestration of reactive oxygen species (40). In our study, *Eif2ak4*-mutated animals did not show exacerbated lung inflammation, at least in term of recruited leukocytes in BAL (supplemental materials). In contrast, these rats showed increased production of TGF-β1 in BAL following BM. This feature was corroborated in endothelial cells cultured from control human lungs and stimulated *in vitro* with BM, which also tended to produce more TGF-β1 upon GCN2 inhibition. Furthermore, increased canonical TGFβ1 signalling (15) has been reported in human and experimental PVOD (41). Considering these data and the major role of TGF-β1 in fibrogenesis, this pathway could contribute, at least in part, to the extensive remodelling of the lung parenchyma and vessels from *Eif2ak4*-mutated animals.

GCN2 protein was detected in our study in both smooth muscle and endothelium from small arteries. In addition, GCN2 was selectively decreased in the endothelium from PF and PF-PH patients, independently of the severity of PH, suggesting that this defect could represent an early feature of vascular pathology during pulmonary remodelling and PF. Microvascular remodeling was also exacerbated in BM-GCN2$^{\Delta 41/\Delta 41}$ animals, leading to increased PH. Although an indirect mechanism linking PF to PH remains possible, these observations point to GCN2 pathway in endothelial cells as a gatekeeper of vascular homeostasis during chronic lung injury. Accordingly, the presence of extravascular blood in the lung alveoli from *Eif2ak4*-mutated rats instilled with BM prompted to determine alveolar-capillary permeability, which was increased in those animals. Interestingly, lung permeability has been correlated with poorer

345 survival in patients with PF (42). Similarly, GCN2$^{-/-}$ mice with dextran sodium sulfate-induced
346 colitis display increased intestinal permeability due to impaired epithelial barrier (40). In the
347 lung, endothelial barrier integrity is increasingly implicated in the pathophysiology of PF by
348 potentially establishing and amplifying the pro-fibrotic environment (43). In addition, our study
349 shows that CD31 expression, a regulator of endothelial junctional integrity (44), was decreased
350 in both human and experimental PF – possibly following the inflammatory response (42) – and
351 an overall reduction in the expression of ZO-1, a tight junctional protein operating downstream
352 of VE-cadherin, was also observed in the endothelium, indicating a loss of the endothelial
353 barrier function following disruption of GCN2 signaling. Interestingly, we found a specific
354 trend towards increased *Il6* mRNA expression in concert with an augmented interleukin (IL)-6
355 release in endothelial cells treated with both BM and the GCN2 inhibitor when compared to
356 BM alone. IL-6 is known to promote endothelial barrier dysfunction via STAT3
357 phosphorylation (45). Moreover, this loss in barrier integrity has not only been linked with
358 alteration in the cytoskeleton, but also with ZO-1 delocalization (46). Furthermore, IL-6
359 production has been associated not only with pulmonary hypertension (47) and pulmonary
360 vascular remodeling (48), but also with pulmonary fibrosis (49) in both animal models and
361 humans (50, 51). It has also been demonstrated that suppression of GCN2 activity in
362 plasmocytoid cells is able to increase cellular IL-6 production (52).

363 The link between GCN2 dysregulation and vascular disease at the (endothelial) cellular level
364 (24) could relate to several mechanisms, including aberrant crosstalk with BMP signaling (15,
365 53), increased proliferation and resistance to apoptosis (13), as well as inflammation, notably
366 through enhanced translation of GM-CSF (54). Our study indicates that GCN2 disruption could
367 also lead to endothelial-to-mesenchymal transition (EndoMT), as the response of endothelial
368 cells which tended to upregulate TGF-β1 and TWIST1 (55, 56) following BM stimulation, was
369 aggravated upon GCN2 inhibition in human control cells. Thus, the study of the role of GCN2

signalling in endothelial homeostasis should be further explored in cells from patients with chronic parenchymal (PF) and/or vascular pathology (PH). A second limitation of this study relates to the end-stage nature of the human pathology (i.e. lung explants), which might favor non-specific findings. This cohort of patients and samples, which was very difficult to collect, provided however consistent findings with our animal model. Whether other pathways are cross-talking with GCN2, such as WNT and mTOR (57) should also be specifically addressed in future studies. Finally, ambiguous results could relate to the fact that a loss-of-function mutation for GCN2 may elicit different downstream signalling when compared with GCN2 inhibition, as already reported for other kinases (58).

In summary, our data in both PF patients and experimental PF consistently indicate that disruption of GCN2 signalling, which is downregulated in the pulmonary endothelium in that situation, leads to aggravation of vascular remodelling and pulmonary fibrosis, probably by connecting endothelial dysfunction, pro-fibrotic signalling and persistent capillary leak. Importantly, those observations recapitulate a frequent phenotype of chronic pulmonary fibrosis with remodeling of both parenchymal and vascular tissues, therefore we propose that restoration of GCN2 signaling represents a candidate strategy for future therapy of PF and PF-PH.

Author Contributions

DSR performed most of the experiments, analysis and drafted the paper; ML provided technical know-how and help with cell cultures and tissue processing; MDB performed conventional histological staining; SV participated in the collection of lung tissue samples for culture and provided lung tissues for biomolecular analysis and immunohistochemistry; CB provided technical know-how and help with the quantification of immunohistochemistry; JA analyzed single cell RNA-seq databases; PD helped with venous and arterial remodeling analysis; YY performed HPLC for hydroxyproline; FH and RQ shared technical knowledge for the bleomycin model and cell culture, respectively; HKQ provided some tissue for

immunohistochemistry; FS provided the *Eif2ak4*-mutated rats; SH shared all the equipment necessary for the cardiovascular evaluation of the animals; DSR, FP, LG and CP designed the study; LG and CP reviewed the data and the writing of this manuscript.

Acknowledgments

The Authors thank the Imaging Platform 2IP (IREC, UCLouvain) for sharing their facility; Prof N. van Baren (Ludwig Institute for Cancer Research of the Duve Institute, UCLouvain, Brussels) for sharing their 3DHistech Pannoramic P250 Flash III digital microscope and their Zeiss Mirax Midi; Prof E. Hermans and his team (Institute Of NeuroScience, UCLouvain, Brussels) for kindly sharing their animal facility resources; the pole of Microbiology (IREC, UCLouvain) for sharing their molecular biology facility; F. Carlier for organizing patients database; F.N. Aboubakar for sharing technical expertise on tyramide multiplex immunochemistry. B. Rondelet (CHU Mont-Godinne, Belgium) and M.R. Ghigna (Hôpital Marie Lannelongue) for their collaboration in lung tissue sampling, and B. Tielemans (KU Leuven, Belgium) for kindly sharing his expertise for the isolation of pulmonary EC.

Funding

DSR was supported by the Fonds National de la Recherche Scientifique (FNRS) – Fonds pour la Recherche dans l'Industrie et l'Agriculture (FRIA, grant 1.E022.17), Belgium, and by the Fonds P. de Merre (Fondation Louvain, grant M1.21221.002). CP is postdoctoral specialist of the FNRS (grants 1.R016.16 and 1.R016.18), Belgium. The study was also supported by a grant to LG from the Fondation Mont-Godinne 2017-2018, Belgium.

References

1. Noble PW, Barkauskas CE, and Jiang D. Pulmonary fibrosis: patterns and perpetrators. *J Clin Invest.* 2012;122(8):2756-62.
2. Richeldi L, Collard HR, and Jones MG. Idiopathic pulmonary fibrosis. *Lancet.* 2017;389(10082):1941-52.
3. Seeger W, Adir Y, Barbera JA, Champion H, Coghlan JG, Cottin V, et al. Pulmonary hypertension in chronic lung diseases. *J Am Coll Cardiol.* 2013;62(25 Suppl):D109-16.
4. Rabinovitch M. Molecular pathogenesis of pulmonary arterial hypertension. *J Clin Invest.* 2012;122(12):4306-13.
5. Simonneau G, Montani D, Celermajer DS, Denton CP, Gatzoulis MA, Krowka M, et al. Haemodynamic definitions and updated clinical classification of pulmonary hypertension. *Eur Respir J.* 2019;53(1).
6. Prins KW, Rose L, Archer SL, Pritzker M, Weir EK, Kazmirczak F, et al. Disproportionate Right Ventricular Dysfunction and Poor Survival in Group 3 Pulmonary Hypertension. *Am J Respir Crit Care Med.* 2018;197(11):1496-9.
7. Barbera JA, and Blanco I. Management of Pulmonary Hypertension in Patients with Chronic Lung Disease. *Curr Hypertens Rep.* 2015;17(8):62.
8. Corte TJ, Keir GJ, Dimopoulos K, Howard L, Corris PA, Parfitt L, et al. Bosentan in pulmonary hypertension associated with fibrotic idiopathic interstitial pneumonia. *Am J Respir Crit Care Med.* 2014;190(2):208-17.
9. Santos-Ribeiro D, Godinas L, Pilette C, and Perros F. The integrated stress response system in cardiovascular disease. *Drug Discov Today.* 2018;23(4):920-9.
10. Eyries M, Montani D, Girerd B, Perret C, Leroy A, Lonjou C, et al. EIF2AK4 mutations cause pulmonary veno-occlusive disease, a recessive form of pulmonary hypertension. *Nat Genet.* 2014;46(1):65-9.
11. Klinger JR. Group III Pulmonary Hypertension: Pulmonary Hypertension Associated with Lung Disease: Epidemiology, Pathophysiology, and Treatments. *Cardiol Clin.* 2016;34(3):413-33.
12. Colombat M, Mal H, Groussard O, Capron F, Thabut G, Jebrak G, et al. Pulmonary vascular lesions in end-stage idiopathic pulmonary fibrosis: Histopathologic study on lung explant specimens and correlations with pulmonary hemodynamics. *Hum Pathol.* 2007;38(1):60-5.
13. Perros F, Gunther S, Ranchoux B, Godinas L, Antigny F, Chaumais MC, et al. Mitomycin-Induced Pulmonary Veno-Occlusive Disease: Evidence From Human Disease and Animal Models. *Circulation.* 2015;132(9):834-47.
14. Selvarajah B, Azuelos I, Plate M, Guillotin D, Forty EJ, Contento G, et al. mTORC1 amplifies the ATF4-dependent de novo serine-glycine pathway to supply glycine during TGF-beta1-induced collagen biosynthesis. *Sci Signal.* 2019;12(582).
15. Manaud G, Nossent EJ, Lambert M, Ghigna MR, Boet A, Vinhas MC, et al. Comparison of Human and Experimental Pulmonary Veno-Occlusive Disease. *Am J Respir Cell Mol Biol.* 2020.
16. Stuart T, Butler A, Hoffman P, Hafemeister C, Papalexi E, Mauck WM, 3rd, et al. Comprehensive Integration of Single-Cell Data. *Cell.* 2019;177(7):1888-902 e21.
17. Habermann AC, Gutierrez AJ, Bui LT, Yahn SL, Winters NI, Calvi CL, et al. Single-cell RNA sequencing reveals profibrotic roles of distinct epithelial and mesenchymal lineages in pulmonary fibrosis. *Sci Adv.* 2020;6(28):eaba1972.
18. Reyfman PA, Walter JM, Joshi N, Anekalla KR, McQuattie-Pimentel AC, Chiu S, et al. Single-Cell Transcriptomic Analysis of Human Lung Provides Insights into the Pathobiology of Pulmonary Fibrosis. *Am J Respir Crit Care Med.* 2019;199(12):1517-36.
19. Garcia-Morales LJ, Chen NY, Weng T, Luo F, Davies J, Philip K, et al. Altered Hypoxic-Adenosine Axis and Metabolism in Group III Pulmonary Hypertension. *Am J Respir Cell Mol Biol.* 2016;54(4):574-83.

20. Nathan SD, Noble PW, and Tuder RM. Idiopathic pulmonary fibrosis and pulmonary hypertension: connecting the dots. *Am J Respir Crit Care Med.* 2007;175(9):875-80.
21. Nossent EJ, Antigny F, Montani D, Bogaard HJ, Ghigna MR, Lambert M, et al. Pulmonary vascular remodeling patterns and expression of general control nonderepressible 2 (GCN2) in pulmonary veno-occlusive disease. *J Heart Lung Transplant.* 2018;37(5):647-55.
22. Dey S, Baird TD, Zhou D, Palam LR, Spandau DF, and Wek RC. Both transcriptional regulation and translational control of ATF4 are central to the integrated stress response. *J Biol Chem.* 2010;285(43):33165-74.
23. Averous J, Lambert-Langlais S, Mesclon F, Carraro V, Parry L, Jousse C, et al. GCN2 contributes to mTORC1 inhibition by leucine deprivation through an ATF4 independent mechanism. *Sci Rep.* 2016;6:27698.
24. Emanuelli G, Nassehzadeh-Tabriz N, Morrell NW, and Marciniak SJ. The integrated stress response in pulmonary disease. *Eur Respir Rev.* 2020;29(157).
25. Lehman SL, Ryeom S, and Koumenis C. Signaling through alternative Integrated Stress Response pathways compensates for GCN2 loss in a mouse model of soft tissue sarcoma. *Sci Rep.* 2015;5:11781.
26. Lu Z, Xu X, Fassett J, Kwak D, Liu X, Hu X, et al. Loss of the eukaryotic initiation factor 2alpha kinase general control nonderepressible 2 protects mice from pressure overload-induced congestive heart failure without affecting ventricular hypertrophy. *Hypertension.* 2014;63(1):128-35.
27. Pereira CM, Filev R, Dubiela FP, Brandao BB, Queiroz CM, Ludwig RG, et al. The GCN2 inhibitor IMPACT contributes to diet-induced obesity and body temperature control. *PLoS One.* 2019;14(6):e0217287.
28. Iglarz M, Landskroner K, Bauer Y, Vercauteren M, Rey M, Renault B, et al. Comparison of Macitentan and Bosentan on Right Ventricular Remodeling in a Rat Model of Non-vasoreactive Pulmonary Hypertension. *J Cardiovasc Pharmacol.* 2015;66(5):457-67.
29. Jarman ER, Khambata VS, Yun Ye L, Cheung K, Thomas M, Duggan N, et al. A translational preclinical model of interstitial pulmonary fibrosis and pulmonary hypertension: mechanistic pathways driving disease pathophysiology. *Physiol Rep.* 2014;2(9).
30. Milara J, Ballester B, Morell A, Ortiz JL, Escriva J, Fernandez E, et al. JAK2 mediates lung fibrosis, pulmonary vascular remodelling and hypertension in idiopathic pulmonary fibrosis: an experimental study. *Thorax.* 2018;73(6):519-29.
31. Arriazu E, Ruiz de Galarreta M, Lopez-Zabalza MJ, Leung TM, Nieto N, and Iraburu MJ. GCN2 kinase is a key regulator of fibrogenesis and acute and chronic liver injury induced by carbon tetrachloride in mice. *Lab Invest.* 2013;93(3):303-10.
32. Krupsky M, Kuang PP, and Goldstein RH. Regulation of type I collagen mRNA by amino acid deprivation in human lung fibroblasts. *J Biol Chem.* 1997;272(21):13864-8.
33. Rishikof DC, Ricupero DA, Poliks CF, and Goldstein RH. Amino acid availability regulates type I procollagen accumulation in human lung fibroblasts. *J Cell Biochem.* 1999;75(1):130-7.
34. Wek SA, Zhu S, and Wek RC. The histidyl-tRNA synthetase-related sequence in the eIF-2 alpha protein kinase GCN2 interacts with tRNA and is required for activation in response to starvation for different amino acids. *Mol Cell Biol.* 1995;15(8):4497-506.
35. Dong J, Qiu H, Garcia-Barrio M, Anderson J, and Hinnebusch AG. Uncharged tRNA activates GCN2 by displacing the protein kinase moiety from a bipartite tRNA-binding domain. *Mol Cell.* 2000;6(2):269-79.
36. Zhang P, McGrath BC, Reinert J, Olsen DS, Lei L, Gill S, et al. The GCN2 eIF2alpha kinase is required for adaptation to amino acid deprivation in mice. *Mol Cell Biol.* 2002;22(19):6681-8.
37. Bringardner BD, Baran CP, Eubank TD, and Marsh CB. The role of inflammation in the pathogenesis of idiopathic pulmonary fibrosis. *Antioxid Redox Signal.* 2008;10(2):287-301.
38. Dorfmuller P, Perros F, Balabanian K, and Humbert M. Inflammation in pulmonary arterial hypertension. *Eur Respir J.* 2003;22(2):358-63.

39. Ravishankar B, Liu H, Shinde R, Chaudhary K, Xiao W, Bradley J, et al. The amino acid sensor GCN2 inhibits inflammatory responses to apoptotic cells promoting tolerance and suppressing systemic autoimmunity. *Proc Natl Acad Sci U S A.* 2015;112(34):10774-9.
40. Ravindran R, Loebbermann J, Nakaya HI, Khan N, Ma H, Gama L, et al. The amino acid sensor GCN2 controls gut inflammation by inhibiting inflammasome activation. *Nature.* 2016;531(7595):523-7.
41. Piersma B, Bank RA, and Boersema M. Signaling in Fibrosis: TGF-beta, WNT, and YAP/TAZ Converge. *Front Med (Lausanne).* 2015;2:59.
42. McKeown S, Richter AG, O'Kane C, McAuley DF, and Thickett DR. MMP expression and abnormal lung permeability are important determinants of outcome in IPF. *Eur Respir J.* 2009;33(1):77-84.
43. Probst CK, Montesi SB, Medoff BD, Shea BS, and Knipe RS. Vascular Permeability in the Fibrotic Lung. *Eur Respir J.* 2020.
44. Privratsky JR, and Newman PJ. PECAM-1: regulator of endothelial junctional integrity. *Cell Tissue Res.* 2014;355(3):607-19.
45. Alsaffar H, Martino N, Garrett JP, and Adam AP. Interleukin-6 promotes a sustained loss of endothelial barrier function via Janus kinase-mediated STAT3 phosphorylation and de novo protein synthesis. *Am J Physiol Cell Physiol.* 2018;314(5):C589-C602.
46. Desai TR, Leeper NJ, Hynes KL, and Gewertz BL. Interleukin-6 causes endothelial barrier dysfunction via the protein kinase C pathway. *J Surg Res.* 2002;104(2):118-23.
47. Hashimoto-Kataoka T, Hosen N, Sonobe T, Arita Y, Yasui T, Masaki T, et al. Interleukin-6/interleukin-21 signaling axis is critical in the pathogenesis of pulmonary arterial hypertension. *Proc Natl Acad Sci U S A.* 2015;112(20):E2677-86.
48. Tamura Y, Phan C, Tu L, Le Hiress M, Thuillet R, Jutant EM, et al. Ectopic upregulation of membrane-bound IL6R drives vascular remodeling in pulmonary arterial hypertension. *J Clin Invest.* 2018;128(5):1956-70.
49. Dawson RE, Jenkins BJ, and Saad MI. IL-6 family cytokines in respiratory health and disease. *Cytokine.* 2021;143:155520.
50. Hu L, Yu Y, Huang H, Fan H, Hu L, Yin C, et al. Epigenetic Regulation of Interleukin 6 by Histone Acetylation in Macrophages and Its Role in Paraquat-Induced Pulmonary Fibrosis. *Front Immunol.* 2016;7:696.
51. Le TT, Karmouty-Quintana H, Melicoff E, Le TT, Weng T, Chen NY, et al. Blockade of IL-6 Trans signaling attenuates pulmonary fibrosis. *J Immunol.* 2014;193(7):3755-68.
52. Sharma MD, Hou DY, Liu Y, Koni PA, Metz R, Chandler P, et al. Indoleamine 2,3-dioxygenase controls conversion of Foxp3+ Tregs to TH17-like cells in tumor-draining lymph nodes. *Blood.* 2009;113(24):6102-11.
53. Malzer E, Dominicus CS, Chambers JE, Dickens JA, Mookerjee S, and Marciniak SJ. The integrated stress response regulates BMP signalling through effects on translation. *BMC Biol.* 2018;16(1):34.
54. Sawada H, Saito T, Nickel NP, Alastalo TP, Glotzbach JP, Chan R, et al. Reduced BMPR2 expression induces GM-CSF translation and macrophage recruitment in humans and mice to exacerbate pulmonary hypertension. *J Exp Med.* 2014;211(2):263-80.
55. Mahmoud MM, Kim HR, Xing R, Hsiao S, Mammoto A, Chen J, et al. TWIST1 Integrates Endothelial Responses to Flow in Vascular Dysfunction and Atherosclerosis. *Circ Res.* 2016;119(3):450-62.
56. Fan Y, Gu X, Zhang J, Sinn K, Klepetko W, Wu N, et al. TWIST1 Drives Smooth Muscle Cell Proliferation in Pulmonary Hypertension via Loss of GATA-6 and BMPR2. *Am J Respir Crit Care Med.* 2020;202(9):1283-96.
57. Karner CM, Esen E, Okunade AL, Patterson BW, and Long F. Increased glutamine catabolism mediates bone anabolism in response to WNT signaling. *J Clin Invest.* 2015;125(2):551-62.

58. Aboubakar Nana F, Lecocq M, Ladjemi MZ, Detry B, Dupasquier S, Feron O, et al. Therapeutic Potential of Focal Adhesion Kinase Inhibition in Small Cell Lung Cancer. *Mol Cancer Ther.* 2019;18(1):17-27.

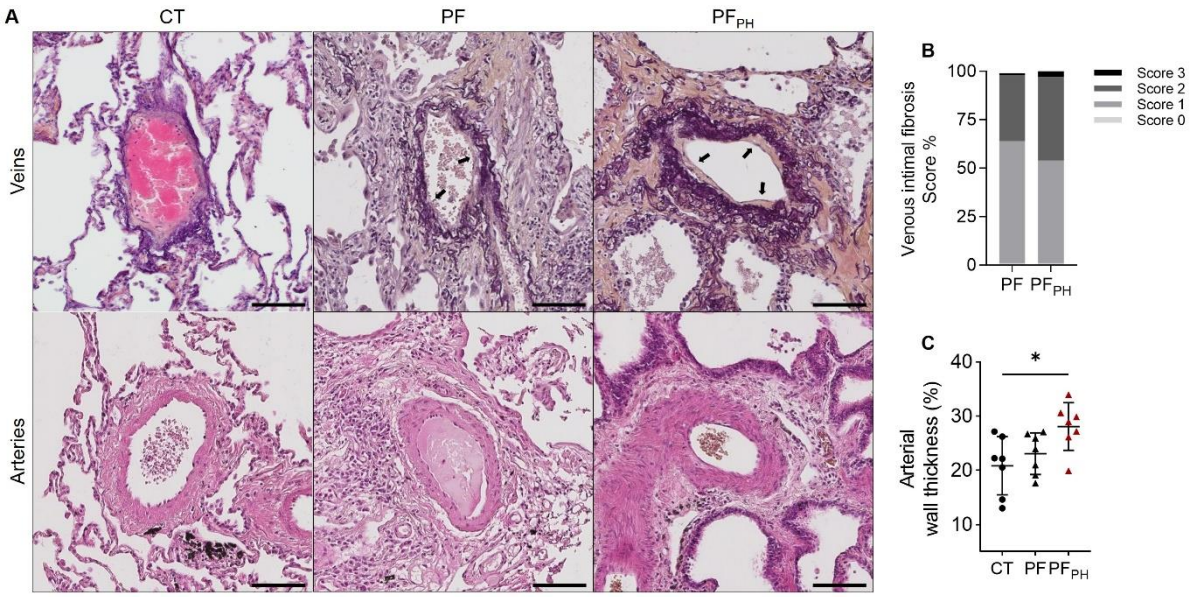

Figure 1. Pulmonary veins and arteries in PF and PF-PH patients. A) Representative veins (top row, hematoxylin-eosin-elastica-saffron stained histological sections) and arteries (bottom row, hematoxylin-eosin stained histological sections) from control (CT), PF and PF-PH patients. **B)** Venous intimal fibrosis score percentage (score 0: intimal fibrosis absent; score 1: mild intimal fibrosis; score 2: moderate intimal fibrosis; score 3: severe intimal fibrosis), p=0.1874, Fisher's test. **C)** Arterial media wall thickness percentage in the same three groups. Scale bar, 100µm. Abbreviations: CT, control; PF, pulmonary fibrosis; PF-PH, pulmonary fibrosis with pulmonary hypertension.

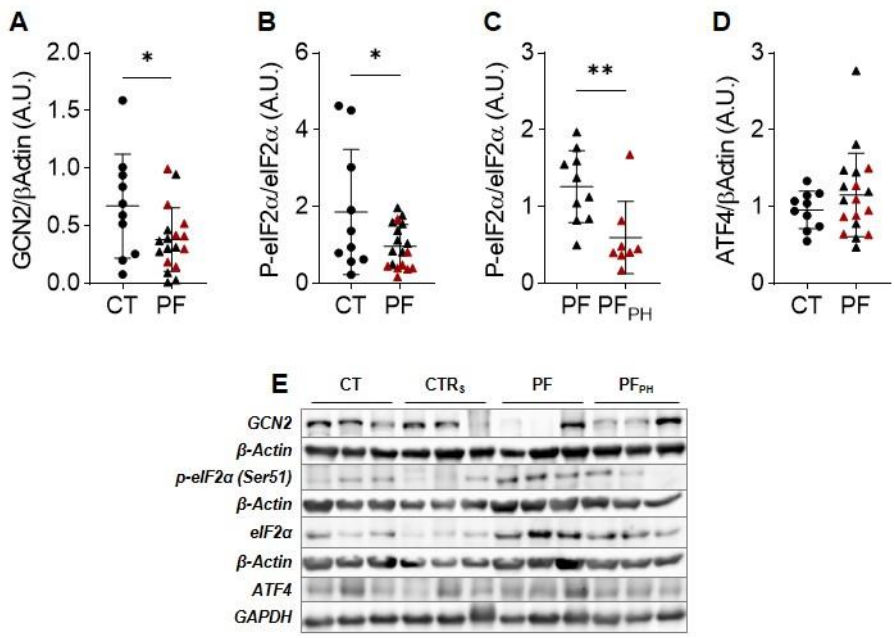

Figure 2. Downregulated GCN2 signaling in human PF and PF-PH lung tissue. A) GCN2 protein expression and **B)** phosphorylated eIF2α at Ser51 measured by western blot in control (CT) (black dots), PF (black triangles) and PF-PH (red triangles) lung tissue lysates. **C)** Phosphorylated eIF2α at Ser51 in PF versus PF-PH lung tissue lysate. **D)** ATF4 protein expression measured by western blot in CT, PF and PF-PH. **E)** Representative western blots in which β-Actin and GAPDH were used as internal controls. Scatter plots indicate mean±SD. *p<0.05, **p<0.01. Abbreviations: ATF4, activating transcription factor 4; CT, control subjects; CTs, control smokers; eIF2α, alpha subunit of the eukaryotic initiation factor 2; GCN2, general control non-derepressible 2; PF, pulmonary fibrosis patients; PF-PH, patients with combined pulmonary fibrosis and pulmonary hypertension.

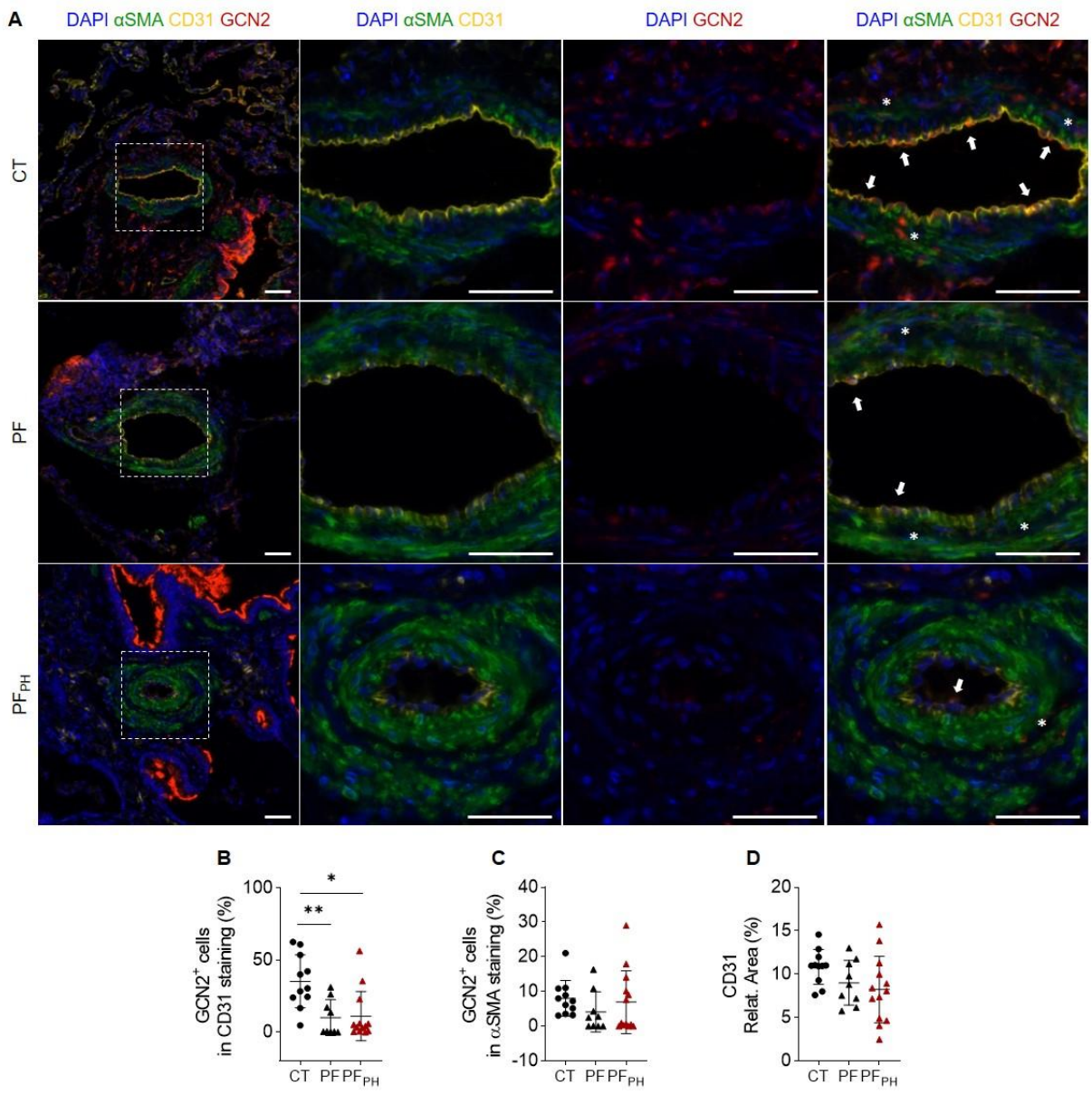

Figure 3. Reduced endothelial GCN2 staining in small lung arteries of patients with PF and PF-PH. A) Representative arteries from control (CT), PF and PF-PH patients. Quadruple immunofluorescence shows strong immunostaining of GCN2 in CD31-positive endothelium (arrows) and in αSMA-positive smooth muscle cells (asterisks) in a small pulmonary artery from a CT) subject. The dashed boxes in the overview images on the first column indicate the area that is shown in more detail on the right panels. Scale bar, 50µm. **B)** Percentage of GCN2-positive cells present in CD31-positive endothelial layer in CT (black dots), PF (black triangles) and PF-PH (red triangles) subjects. **(C)** Percentage of GCN2-positive cells present in αSMA-

positive media layer in the three same groups. **(D)** CD31 immunostaining relative area percentage in the lung of PF patients when compared with CT. Nuclear counterstaining with DAPI. Scatter plots indicate mean±SD. *p<0.05; **p<0.01. (B-C: Kruskal-Wallis test and D: one-way ANOVA). Abbreviations: αSMA, alpha smooth muscle actin; GCN2, general control non-derepressible 2.

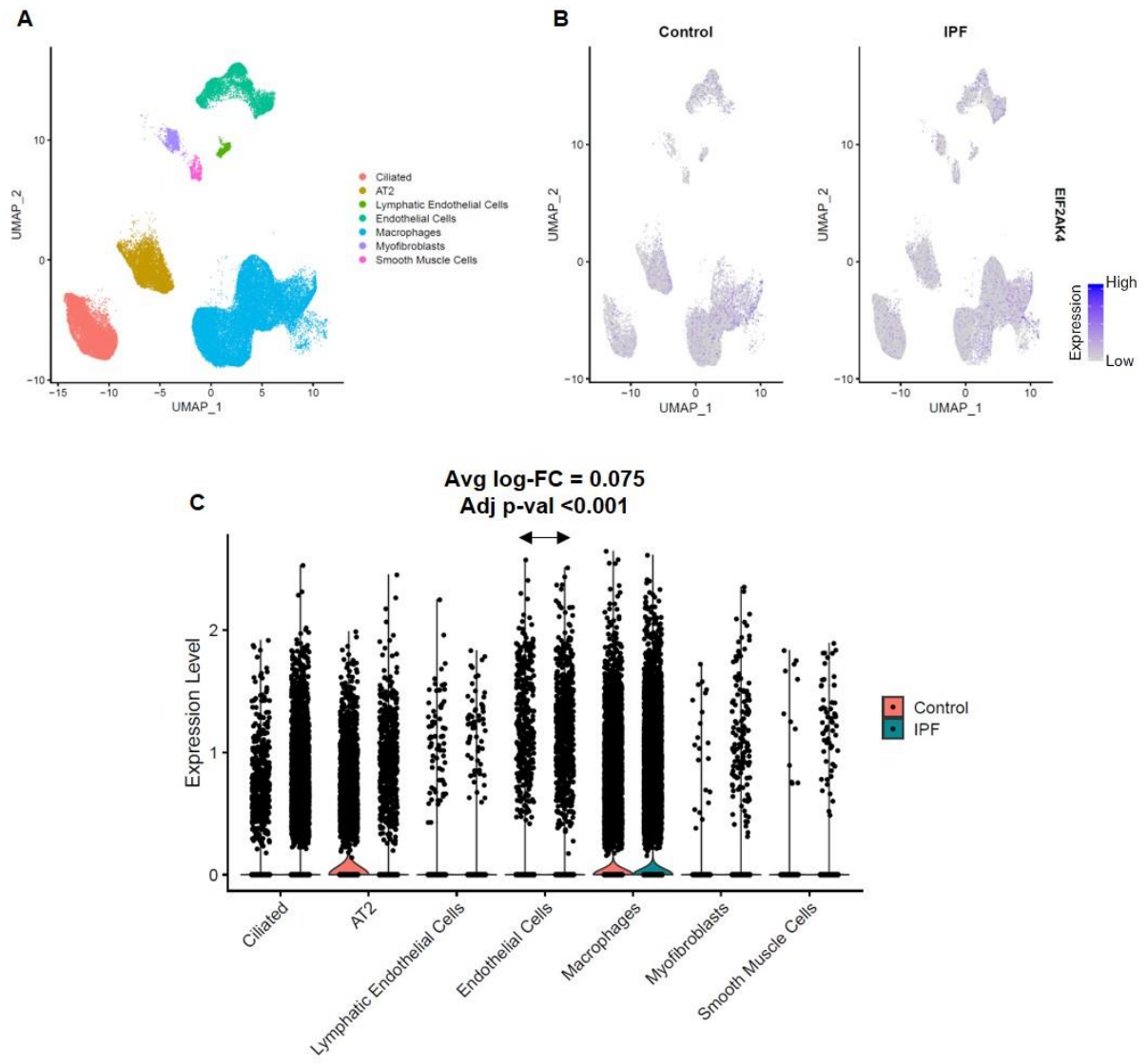

Figure 4. Analysis of *EIF2AK4* expression by single cell RNA-Seq in endothelial cells and other cell types from IPF and control lungs. Single cell RNA-Seq was performed (17) on single-cell suspensions from 20 IPF and 10 non-fibrotic control lungs. **A)** Seven cell populations were selected from the processed data made available by the authors and were illustrated in a Uniform Manifold Approximation and Projection (UMAP) plot. **B)** *EIF2AK4* expression in controls (n=10, on the left) and IPF (n=20, on the right) patients. **C)** Violin plots of *EIF2AK4* expression in controls (n=10, on the left) and IPF patients (n=20, on the right). Average log Fold-Change = 0.075, adjusted p-value <0.001) for *EIF2AK4* expression in endothelial cells from IPF versus controls.

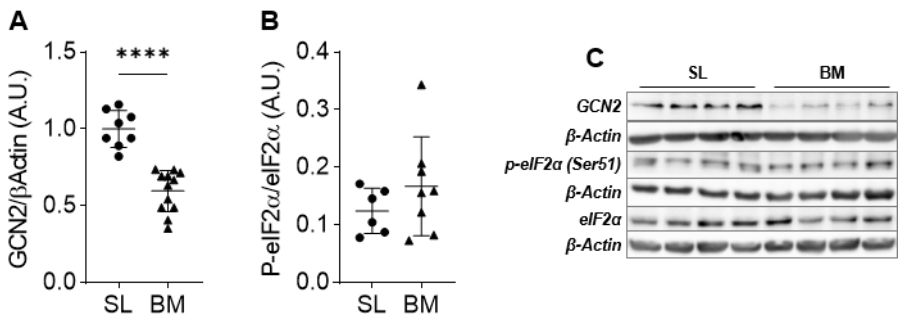

Figure 5. Decreased GCN2 protein expression in an experimental model of combined PF-PH. A) GCN2 protein and **B)** phosphorylated-eIF2α at Ser51 assayed by western blot in lung tissue from rats instillated with bleomycin (BM) as compared with rats instillated with saline (SL). **C)** Representative western blots, in which β-Actin was used to control for equal loading of lanes. Scatter plots indicate mean±SD, *p<0.05, ****p<0.0001. Abbreviations: eIF2α, alpha subunit of the eukaryotic initiation factor 2; GCN2, general control non-derepressible 2.

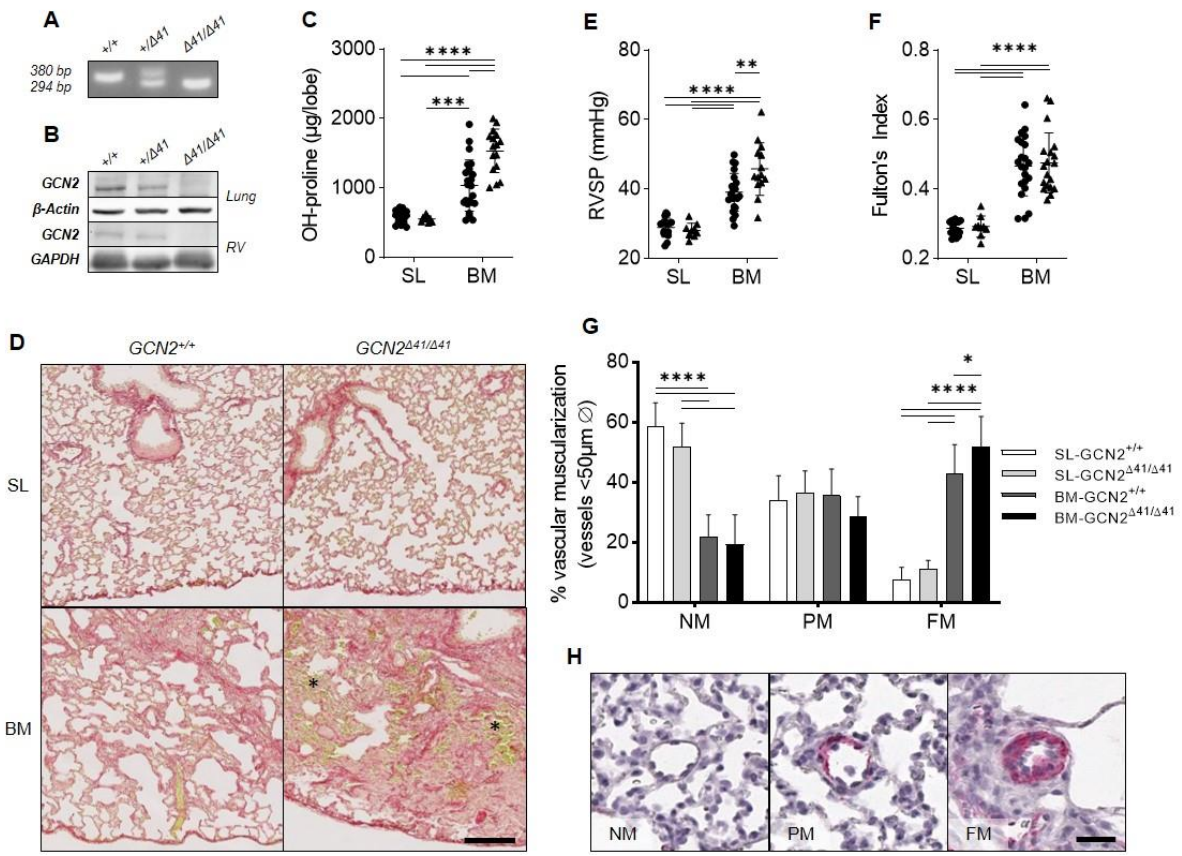

Figure 6. GCN2 loss-of-function mutation aggravates bleomycin-induced pulmonary fibrosis and hypertension. A) Representative agarose gel showing the PCR products generated from DNA from wild-type (WT $GCN2^{+/+}$), heterozygous ($GCN2^{+/\Delta41}$) and homozygous ($GCN2^{\Delta41/\Delta41}$) rats. **B)** Immunoblotting for GCN2 of lung (upper lanes) and right ventricle (RV, lower lanes) homogenates of representative WT, $GCN2^{+/\Delta41}$ and $GCN2^{\Delta41/\Delta41}$ rats. **C)** Hydroxyproline levels in rat lung homogenates measured by HPLC. **D)** Representative Sirius red staining images showing increased collagen deposition within the lung of BM rats, along with the presence of extravascular blood (asterisks). Scale bar, 200µm. **E)** RVSP measured by right heart catheterization. **F)** Fulton's index measured by the weight of the RV normalized for the LV+S weight. **G)** Calculation of the percentage of nonmuscularized (NM), partially muscularized (PM) and fully muscularized (FM) microvessels within the lung of SL and BM rats. **H)** Representative immunohistochemistry images for α-smooth muscle actin (αSMA)

showing the different vascular muscularization categories. Counterstaining with hematoxylin-eosin. Scale bar, 25µm. Scatter plots and bars indicate mean±SD. *p<0.05, **p<0.01, ****p<0.0001. (C, E, F, G: two-way ANOVA). Abbreviations: RVSP, right ventricular systolic pressure.

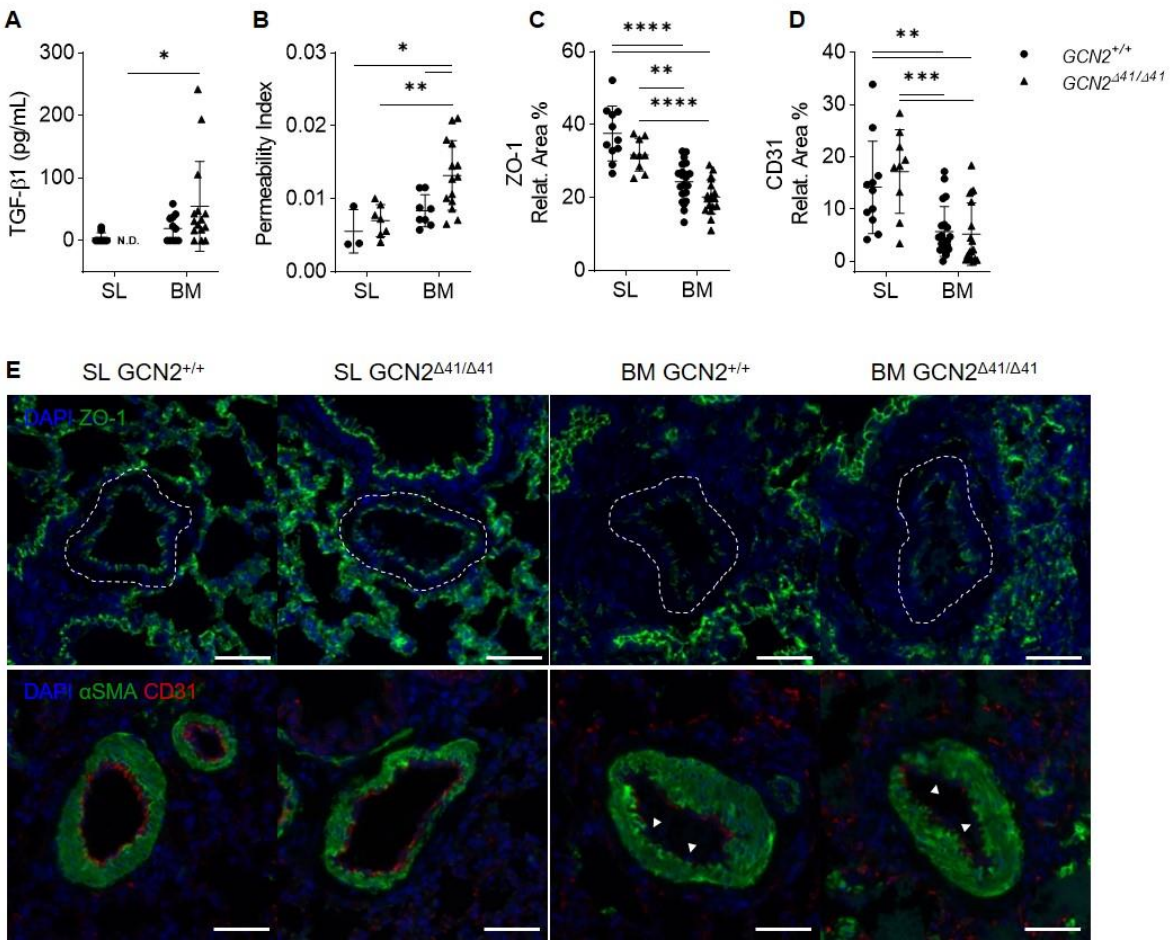

Figure 7. GCN2 loss-of-function leads to increased TGF-β1 production and endothelial hyperpermeability. A) Total TGF-β1 detected in bronchoalveolar lavage (BAL) fluid. **B)** Pulmonary permeability index measured by the ratio between the total protein concentration in the BAL normalized for that in serum. **C)** Zonula Occludens **(**ZO)-1 and **D)** CD31 immunostaining, expressed as the relative area (percentage) in rat pulmonary arteries. E) Representative images for the different experimental groups of a double immunofluorescence of ZO-1 (superior row) and a triple immunofluorescence of αSMA (green) and CD31 (red) (inferior row) in addition to DAPI (nuclear counterstaining, blue). Arrowheads indicate endothelial cells. Scale bar, 50µm. Scatter plots indicate mean±SD. *p<0.05, **p<0.01, ***p<0.001, ****p<0.0001. (A-D: two-way ANOVA). Abbreviations: αSMA, alpha smooth muscle actin; GCN2, general control non-derepressible 2.

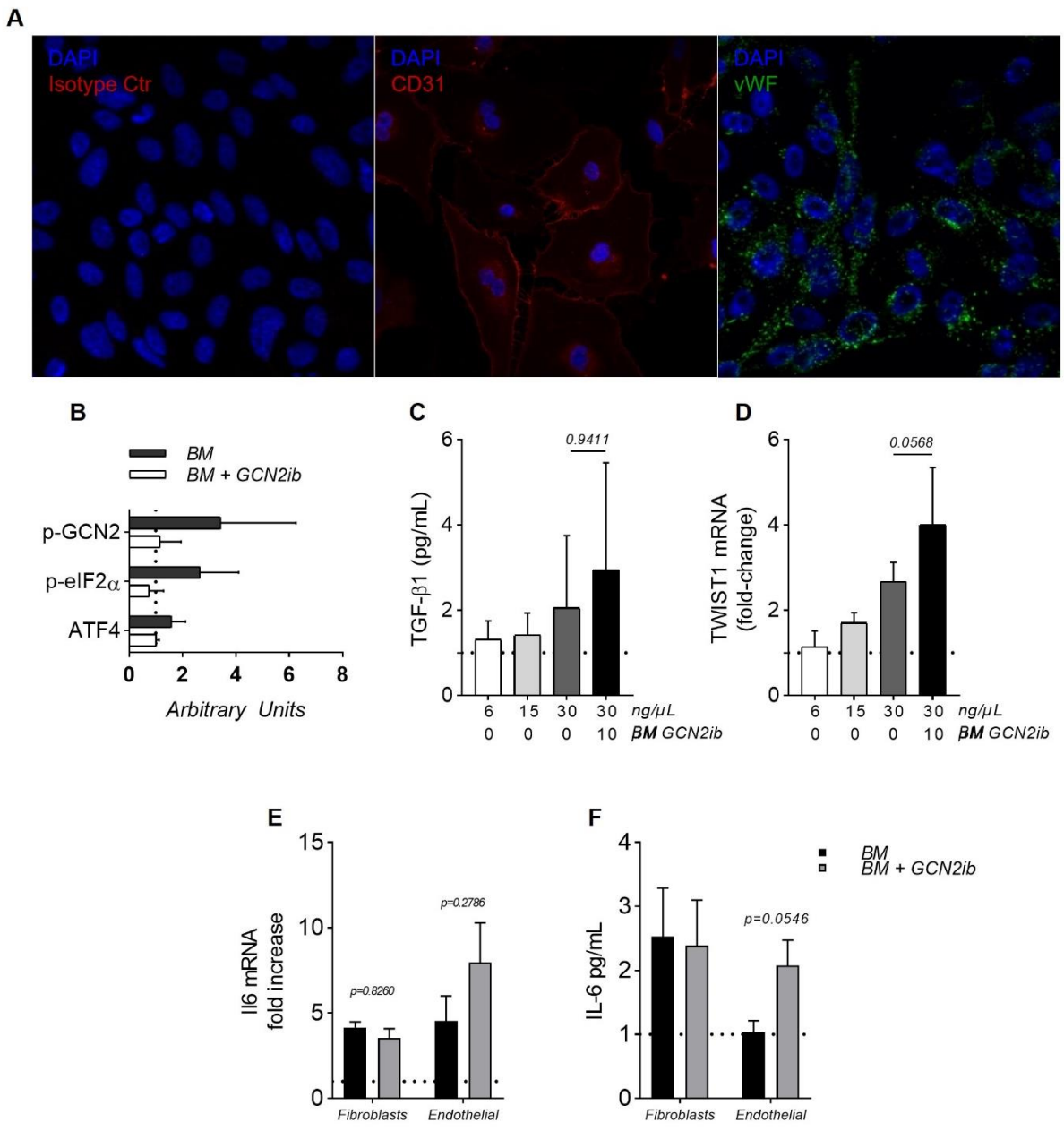

Figure 8. GCN2 inhibition dysregulates endothelial cell response to BM. A) Endothelial cell (EC) characterization, with pulmonary EC isolated from control patients positive for CD31 and von Willebrand factor (vWF). **B)** Phospho-GCN2, p-eIF2α and ATF4 expression in endothelial cells treated with BM with or without GCN2 inhibitor (GCN2ib), as assessed by western blot. **C)** Released TGF-β1 and **D)** TWIST1 expression by endothelial cells treated with BM with or without GCN2 inhibitor. E) *Il-6* mRNA expression and released IL-6 in both fibroblasts and

endothelial cells treated with BM in the absence or presence of GCN2 inhibitor. C and D, one-way ANOVA (n=4 per condition).

832 **TABLE 1.** Characteristics of the patients enrolled in this study at the time of transplantation.

Parameter	**CTR** *(n=14)*	**PF** *(n=13)*	**PF-PH** *(n=12)*	***p value***
Age (years)	53 ± 18	56 ± 11	56 ± 11	*0.8459*
Sex (M/F)	5/9	9/4	5/7	-
Diagnosis	-	*10 IPF* *2 unclassifiable IIP* *1 IIP – UIP pattern*	*5 IPF* *3 unclassifiable IIP* *4 CTD (2UIP, 1 unclassifiable, 1 NSIP)*	-
Smoking history	-	*3 non-smokers* *6 ex-smokers* *4 unknown*	*4 non-smokers* *5 ex-smokers* *3 unknown*	-
Pack-years	-	26 ± 8	21 ± 16	*0.1871*
FVC (% predicted)	133 ± 25	59 ± 23* *p<0.0001*	61 ± 20* *p<0.0001*	*<0.0001*
DLCO (% predicted)	88 ± 16	35 ± 13* *p<0.0074*	28 ± 11* *p<0.0007*	*0.0004*
mPAP (mmHg)	-	18 ± 3	35 ± 9$^{\#}$	*<0.0001*

833 All values are reported as mean±SD. *p<0.05 vs CTR; $^{\#}$p<0.05 vs PF. To compare the following
834 groups: CTR, PF and PF-PH, the statistical tests used were either one-way ANOVA or Kruskal-
835 Wallis test, according to the normality of the data. To compare PF and PF-PH the test used was
836 unpaired t-test. Abbreviations: DLCO, diffusing lung capacity for carbon monoxide; FVC,
837 forced vital capacity; IIP, idiopathic interstitial pneumonia; IPF, idiopathic pulmonary fibrosis;
838 mPAP, mean pulmonary artery pressure; NSIP, non-specific interstitial pneumonia; UIP, usual
839 interstitial pneumonia.

Methods

Human lung samples

Human lung tissue was collected with patient's agreement and ethical approval by UCL (Ref. protocol "CLARA" 2005/22SEP/149 – update 29/11/2016) and KU Leuven (S51577, S52174 and S55877). Control lung tissue was collected from patients undergoing lung resection surgery due to a solitary lung cancer, at distance of the tumoral site following careful evaluation by a pathologist. Lung tissue (explants) was obtained from PF patients undergoing lung transplantation. Presence of PF was based on clinical basis including lung scanning and confirmed by lung histology while PH was determined by right heart catheterization (or estimated by echocardiography, by using the derivation of right ventricular pressure from the tricuspid regurgitation velocity added to a qualitative assessment of right atrial pressure).

Animal experiments and Eif2ak4-mutated rats

Our animal experiments were performed in agreement with the European Community regulations, followed the recommendations of the *Guide for the Care and Use of Laboratory Animals* (NIH publication No. 85-23, revised 2011, US) and were approved by the local ethical committee for animal research at the UCLouvain (2017/UCL/MD/003). These rats were generated on a Sprague Dawley background by using the Zinc-Finger nuclease method, as previously described (1). A frameshift deletion of 41 base pairs (*Eif2ak4*$_{\Delta 41}$) was introduced in the first exon of the *Eif2ak4* gene. The strain developed can be either monoallelic or biallelic. Rats with 3 weeks-old were genotyped using genomic DNA obtained from ear punches.

Five to 6 weeks-old rats weighing approximately 250g were randomly assigned to receive either an intratracheal instillation of 7.5U/kg of bleomycin sulphate (Sanofi) or an equal volume of vehicle (0.9% NaCl, Baxter). Three weeks post-instillation (day 21), animals were submitted to an invasive hemodynamic evaluation, followed by euthanasia through exsanguination and sample collection for histological and molecular studies.

Hemodynamic measurements

At the end of the experimental protocol and after anesthesia, animals underwent an endotracheal intubation and were connected to a rodent ventilator (RoVent, Kent Scientific Corporation) with an animal weight-defined pressure and respiratory rate. Animal's temperature was monitored and regulated by a rectal temperature sensor and a warming pad, respectively. A lower thoracotomy was performed and a pressure catheter (SPR-407, Millar, Houston, USA) was inserted through the apex of the right ventricle (RV) and positioned along the long axis of the heart. The experimental preparation was allowed to stabilize for 10-15 min and then recordings were performed. Pressure signals were continuously acquired (Bridge Amp) and digitally recorded at a sampling rate of 1.000 Hz (ML870 PowerLab 8/30, ADinstruments) and analysed off-line (LabChart 8 Pro, ADinstruments). Baseline hemodynamics parameters were heart rate (HR) and RV pressures.

Sample collection and morphometric analysis

At the end of the hemodynamic assessment and immediately after exsanguination, using the endotracheal tube already in place, the lungs were infused 2 times with 20 mL/kg of chilled 0.9% NaCl. The bronchoalveolar lavage (BAL) was then centrifuged (300g for 5min at 4°C) and the cell-free supernatant was stored for further biochemical studies. Heart and lungs were excised *in bloc*. RV free wall, LV plus septum (LV+S) and lungs were dissected and weighed separately in order to determine the Fulton's index (the ratio between the weight of the RV and the weight of the LV plus septum). The tibia was collected and measured for tissue weight normalization. Organ samples were collected and snap frozen in liquid nitrogen and stored at -80°C. Lung collagen accumulation was estimated by measuring the hydroxyproline (OH-proline) contents by HPLC in lung homogenates as previously described (2).

Histological analysis

After fixation for 48h, histological samples were embedded in paraffin and serial sections of 5µm were obtained from lung tissue. Hematoxylin and eosin (HE), hematoxylin-eosin-elastica-saffron (HEES) and Picrosirius red staining was used to analyze lung remodeling. Sections were scanned using a digital slide scanner (SCN400, Leica Biosystems) and analyzed using the TissueIA software (SlidePath) and Cytomine. Small pulmonary veins (defined as having an outer diameter inferior to 200µm) were distinguished from small pulmonary arteries (also defined as having an outer diameter inferior to 200 µm) based on both position and structure, as previously published (3). Pulmonary veins were characterized according to the following scoring system: score 0, intimal fibrosis absent; score 1, mild intimal fibrosis; score 2, moderate intimal fibrosis; and score 3, severe intimal fibrosis.

Multiplex immunofluorescence staining

Human and rat lung tissue sections were processed as previously described (4). Human tissue sections were submitted to three sequential incubations with an anti-GCN2 antibody (Abcam, Cambridge, UK), GCN2, CD31 and αSMA were revealed with TSA-conjugated fluorophores, AF647, AF555 and AF488, respectively. Rat tissue sections were submitted to two sequential incubations with an anti-CD31 antibody (Abcam) and an anti-αSMA (Santa Cruz Biotechnology, Santa Cruz, CA). CD31 and αSMA were revealed with TSA-conjugated fluorophores, AF647 and AF488, respectively. Finally, sections were counterstained with DAPI and mounted with a Dako fluorescence mounting medium. Negative controls were achieved by adding nonspecific isotype controls as primary antibodies. Multiplex stained whole slides were imaged using a Panoramic 250 Flash digital microscope (P250 FlashIII Digital Microscopes, 3DHISTECH, Budapest, Hungary).

Protein extraction and immunoblotting

Samples were homogenized in cold RIPA lysis buffer (50mM Tris-HCl pH 8, 150mM NaCl, 0.1% Triton X-100, 0.5% sodium deoxycholate and 0.1% SDS) containing protease

(cOmplete™, EDTA-free protease inhibitor cocktail, Roche, Mannheim, Germany) and phosphatase (PhosSTOP, Sigma-Aldrich, Saint-Louis, MO) inhibitors. After centrifugation (15000g for 20 min at 4°C), supernatants were collected and total protein concentration was determined using BCA assay (Sigma-Aldrich) according to manufacturer's instructions. Samples were treated with laemmli loading buffer (31.5mM Tris-HCl pH 6.8, 10% glycerol, 1% SDS, 0.005% bromophenol blue and 355mM 2-mercaptoethanol) and boiled for 5 min at 95°C. Equal amount of protein was loaded onto a SDS-PAGE gel and electroblotted onto a 0.45µm nitrocellulose membrane (Amersham™ Protran, Sigma). Blots were blocked with 5% BSA for 1 hour at RT and incubated overnight at 4°C with primary antibodies to GCN2, eIF2α, p-eIF2α or ATF4). After primary antibody removal, membranes were washed with tris-buffered saline with 0.01% Tween-20 (TBS-T) and incubated with a secondary HRP-conjugated, goat anti-rabbit IgG (Cell Signaling, Danvers, MA) or anti-mouse IgG (Sigma) in 2% BSA for 1 hour at RT. After washing, membranes were imaged with a chemiluminescence system (ChemiDoc™ XRS, Bio-Rad, Hercule, CA) and analyzed using Quantity One 1-D analysis software (Bio-Rad).

ELISA and BCA assay

Total TGF-β1 concentration was measured in acidified BAL by ELISA, according to the manufacturer's instructions (Duoset, R&D systems, Minneapolis, MN). BCA assay was used to measure total proteins in BAL and serum of rats, according to the manufacturer's instructions.

Primary human lung microvascular endothelial cell (HLMEC) culture

EC isolation was performed as previously described (5). Immunomagnetic positive selection of EC was performed using anti-CD31-labeled beads (CD31 MicroBead Kit human, Miltenyi Biotec) according to the manufacturer's instructions. ECs were phenotyped by flow cytometry, by labelling cells with anti-CD31-FITC antibody (Miltenyi Biotec), and by

immunofluorescence using antibodies against CD31 (Abcam) and von Willebrand factor (Dako). All experiments were carried out between passages 3 and 6. EC were treated with BM (6 to 30 ng/μL, Sanofi) for 48h in the presence or not of HY-112654 (10 μM, MedChemExpress, USA), a selective inhibitor of GCN2.

Analysis of single cell RNA-Seq databases for GCN2/EIF2AK4 mRNA expression

Original data was retrieved from two recent publications (6), in which single-cell RNA-Sequencing was performed on single-cell suspensions generated from lung biopsies of transplant donors (or non-fibrotic control lung explants in the case of the former study) and lung explants from transplanted patients with PF. All data were analyzed with Seurat R package (7). In the Reyfman study, cell type assignments were performed based on the R package 'SingleR' (8) using the Human Primary Cell Atlas Database for the latter study (15), while seven cell populations were selected from the processed data made available by the authors of the former study (14).

Statistical analysis

Statistical analysis was performed using GraphPad Prism 8 (GraphPad Software Inc.). Most of the data was analyzed using a t-test or a two-way ANOVA. Exceptions to this were detailed in the figure captions. Single-cell RNA-Seq was analyzed with Seurat R package. All graphs are presented as mean±SD and differences with $p<0.05$ were considered statistically significant.

References

1. Manaud G, Nossent EJ, Lambert M, Ghigna MR, Boet A, Vinhas MC, et al. Comparison of Human and Experimental Pulmonary Veno-Occlusive Disease. *Am J Respir Cell Mol Biol.* 2020.
2. Bondue B, Sherer F, Van Simaeys G, Doumont G, Egrise D, Yakoub Y, et al. PET/CT with 18F-FDG- and 18F-FBEM-labeled leukocytes for metabolic activity and leukocyte recruitment monitoring in a mouse model of pulmonary fibrosis. *J Nucl Med.* 2015;56(1):127-32.
3. Fayyaz AU, Edwards WD, Maleszewski JJ, Konik EA, DuBrock HM, Borlaug BA, et al. Global Pulmonary Vascular Remodeling in Pulmonary Hypertension Associated With Heart Failure and Preserved or Reduced Ejection Fraction. *Circulation.* 2018;137(17):1796-810.
4. Aboubakar Nana F, Hoton D, Ambroise J, Lecocq M, Vanderputten M, Sibille Y, et al. Increased Expression and Activation of FAK in Small-Cell Lung Cancer Compared to Non-Small-Cell Lung Cancer. *Cancers (Basel).* 2019;11(10).
5. Vengethasamy L, Hautefort A, Tielemans B, Belge C, Perros F, Verleden S, et al. BMPRII influences the response of pulmonary microvascular endothelial cells to inflammatory mediators. *Pflugers Arch.* 2016;468(11-12):1969-83.
6. Reyfman PA, Walter JM, Joshi N, Anekalla KR, McQuattie-Pimentel AC, Chiu S, et al. Single-Cell Transcriptomic Analysis of Human Lung Provides Insights into the Pathobiology of Pulmonary Fibrosis. *Am J Respir Crit Care Med.* 2019;199(12):1517-36.
7. Stuart T, Butler A, Hoffman P, Hafemeister C, Papalexi E, Mauck WM, 3rd, et al. Comprehensive Integration of Single-Cell Data. *Cell.* 2019;177(7):1888-902 e21.
8. Aran D, Looney AP, Liu L, Wu E, Fong V, Hsu A, et al. Reference-based analysis of lung single-cell sequencing reveals a transitional profibrotic macrophage. *Nat Immunol.* 2019;20(2):163-72.

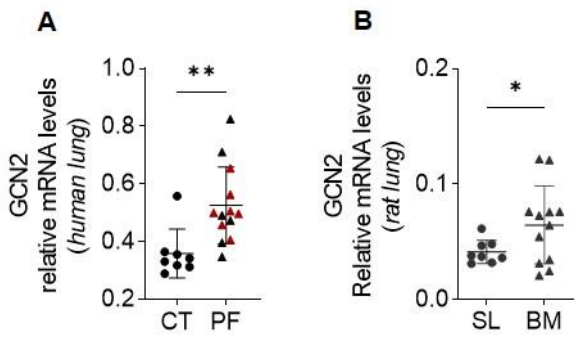

Supplemental Figure 1. Validation RT-qPCR. Increased expression of GCN2 (*EIF2AK4*) mRNA transcripts in lung tissue from patients with PF as compared with control lung tissue (A) and in lung tissue from rats submitted to bleomycin (BM) in comparison with saline (SL) rats (B). Scatter plots indicate mean±SD, *p<0.05 and **p<0.01.

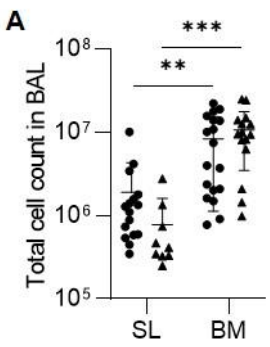

Supplemental Figure 2. Total cell numbers in bronchoalveolar lavage (BAL). Animals instilled with BM showed increased total cell numbers in BAL, regardless of the animal genotype. Scatter plots indicate mean±SD, **p<0.01; ***p<0.001.

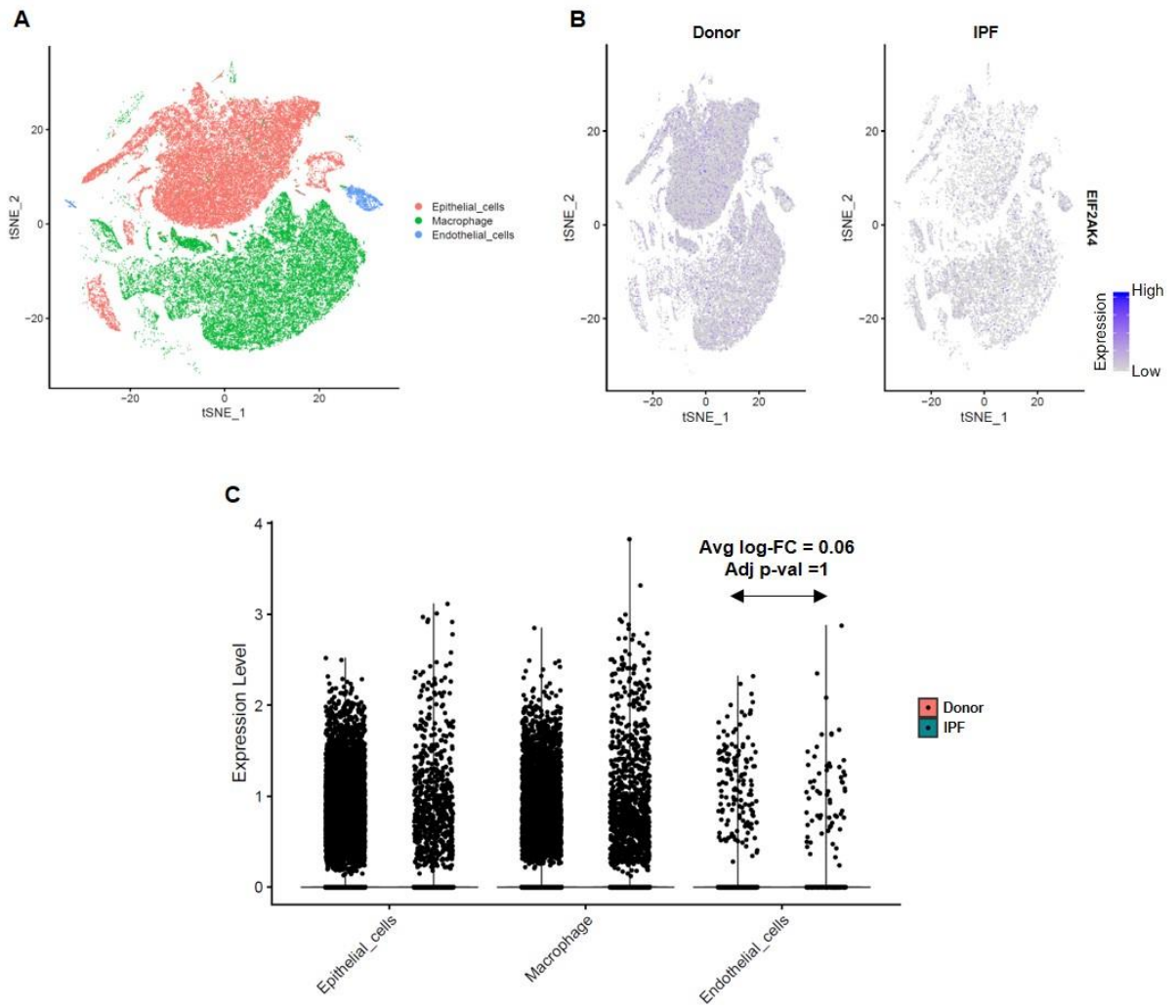

Supplemental Figure 3. Analysis of *EIF2AK4* expression by single cell RNA-Seq in endothelial cells, as compared to macrophages and epithelial cells, in IPF and control lungs. Single cell RNA-Seq was performed (15) on single cell suspensions from transplant donors and IPF lung explants. **A**) Cell type assignments were performed based on the R package 'SingleR' using the Human Primary Cell Atlas Database and three cell populations were selected and illustrated in a t-distributed Stochastic Neighbor Embedding (tSNE) plot. **B)** *EIF2AK4* expression in donor (n=8, on the left) and IPF (n=4, on the right) patients. **C**) Violin plots of EIF2AK4 expression in donor (n=8, on the left) and IPF patients (n=4, on the right). Average log Fold-Change = 0.06, Adjusted p-value =1 for *EIF2AK4* expression in endothelial cells from IPF versus donors.

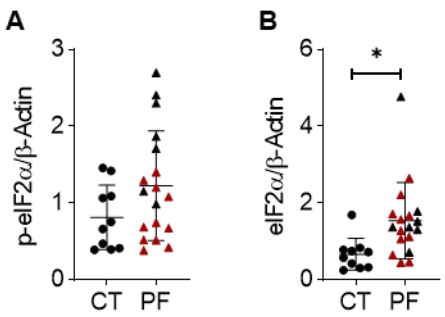

Supplemental Figure 4. EIF2α expression in human lung tissue. A) Phosphorylated eIF2α at Ser51 and B) total eIF2α measured by western blot in control (CT, black dots), PF (black triangles) and PF-PH (red triangles) lung tissue lysates. Scatter plots indicate mean±SD. *p<0.05. Abbreviations: CT, control subjects; eIF2a, alpha subunit of the eukaryotic initiation factor 2; PF, pulmonary fibrosis patients and PF-PH, patients with combined pulmonary fibrosis and pulmonary hypertension.

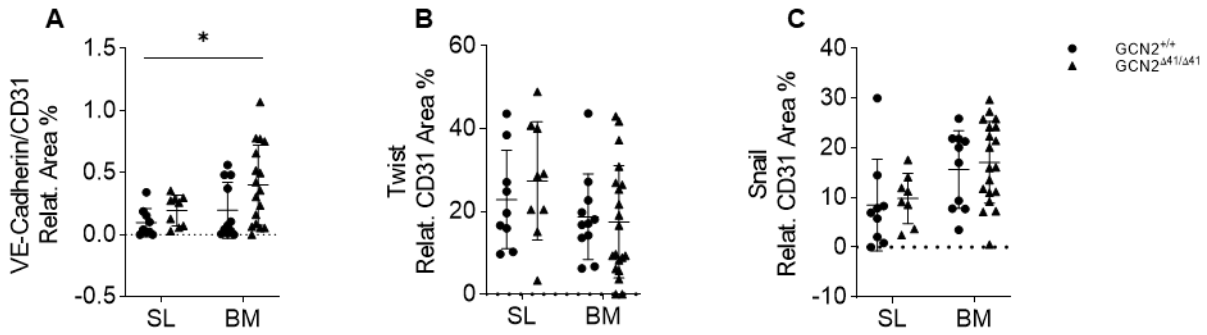

Supplemental Figure 5. Expression of VE-cadherin, Twist and Snail in human lung arteries. A) VE-cadherin B) Twist and c) Snail protein expression in CD31-positive endothelial cells. Scatter plots indicate mean±SD. *p<0.05. Abbreviations: BM, bleomycin; SL, saline.

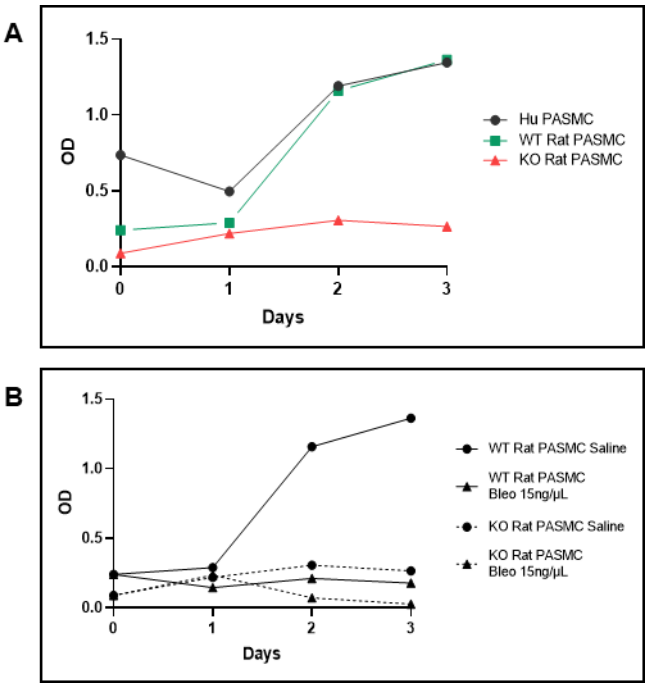

Supplemental Figure 6. Proliferation rate of primary Pulmonary Artery Smooth Muscle Cells isolated from the lung of wild type and mutated rats. A) Proliferation rate of human PASMC in comparison with wild type and mutated rat PASMC in normal conditions and **B**) wild type and mutated rat PASMC submitted to bleomycin treatment, measured by the WST-1 assay (n=1).

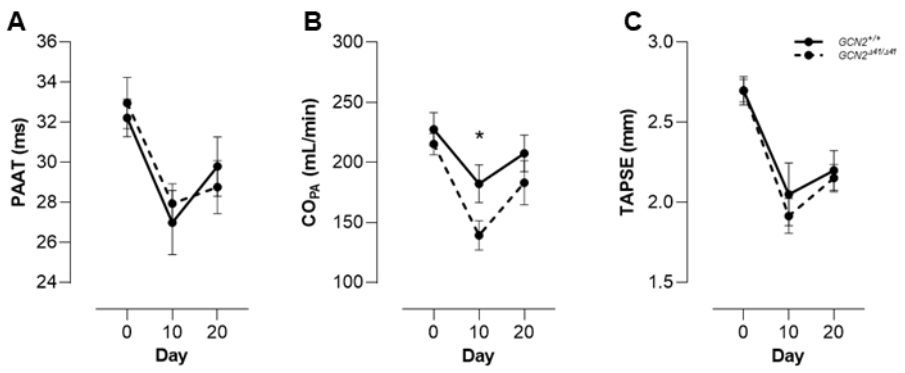

Supplemental Figure 7. Echocardiographic parameters assessed in wild type and mutated animals submitted to bleomycin. A) Pulmonary Artery Acceleration Time, B) Cardiac Output and C) Tricuspid Annulus Peak Systolic Excursion measured in wild type (line) and mutated (dotted line) rats before bleomycin treatment (day 0), 10 and 20 days after bleomycin instillation. Line chart indicate mean±SD. *$p<0.05$.

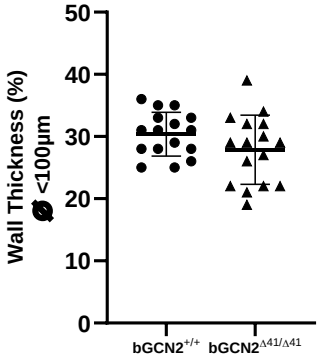

Supplemental Figure 8. Pulmonary arterial remodeling in wild type and mutated rats submitted to bleomycin. Pulmonary artery wall thickness percentage measured in vessels with an outer diameter inferior to 100µm in wild type and mutated rats submitted to bleomycin treatment.

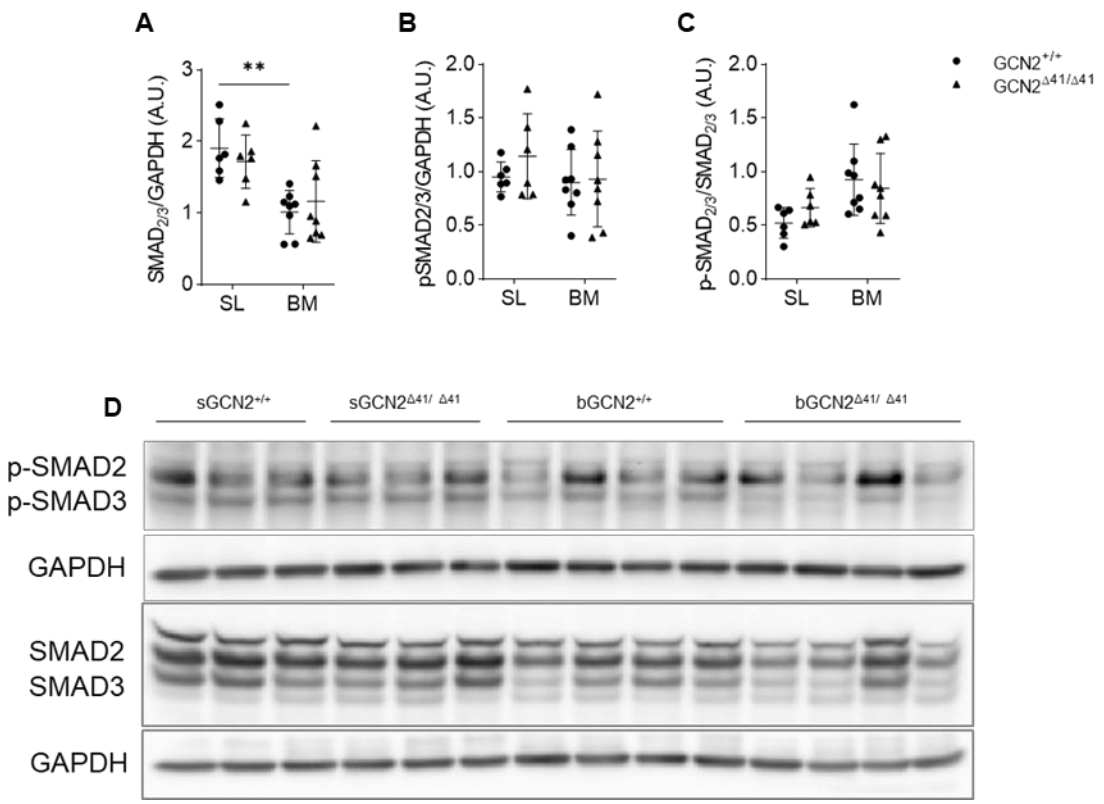

Supplemental Figure 9. Protein expression of SMAD2/3 in the lung of wild type and mutated animals. A) SMAD2/3 and **B)** phosphorylated-SMAD2/3 protein expression normalized to GAPDH and **C)** phosphorylated-SMAD2/3 protein expression normalized to total SMAD2/3 levels. **D)** Representative western blots in which GAPDH was used as internal controls. Scatter plots indicate mean±SD. **p<0.01.

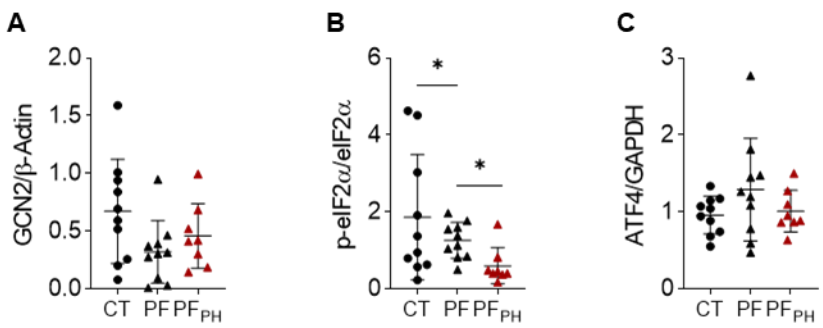

Supplemental Figure 10. Downregulated GCN2 signaling in human PF and PF-PH lung tissue. A) GCN2, B) phosphorylated eIF2α at Ser51 and C) ATF4 protein expression measured by western blot in control (CT) (black dots), PF (black triangles) and PF-PH (red triangles) lung tissue lysates. Scatter plots indicate mean±SD. *p<0.05.

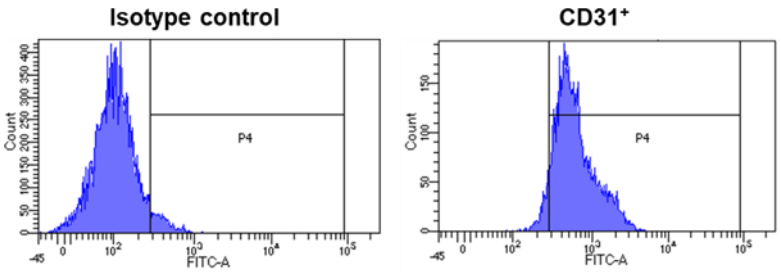

Supplemental Figure 11. Representative PAEC cells analyzed for the presence of CD31 by flow cytometry. Left panel, PAEC cells immuno-labeled with isotype control. Right panel, PAEC cells immuno-labeled with CD31 magnetic beads quantified by flow cytometry.